Minimum Entrainer Flows for Extractive Distillation: a Bifurcation Theoretic Approach

Jeffrey P. Knapp and Michael F. Doherty
Dept. of Chemical Engineering, University of Massachusetts, Amherst, MA 01003

In addition to a minimum reflux, every extractive distillation exhibits a maximum reflux, above which the desired separation is impossible, and a minimum entrainer flow rate, below which the separation is also impossible. Both of these quantities correspond to bifurcations of the finite difference equations describing the middle section of the column and, given a VLE model, can be easily calculated knowing only information about the column feed and the desired product compositions, that is, prior to any column design calculations.

Both maximum reflux and minimum entrainer flows have important implications for the design and operation of extractive distillations. By limiting the range of feasible operating reflux ratios, the maximum reflux affects the flexibility, operability and controllability of the column. Ranking a set of feasible extractive entrainers according to their minimum entrainer flows provides a simple effective method for identifying the most promising candidates. Near optimal design values of the entrainer flow can then be estimated using the heuristic presented.

Introduction

Azeotropic mixtures are normally separated by extractive or azeotropic distillation. In either process, a liquid separating agent is added to facilitate the separation. For extractive distillation, the separating agent is the heaviest species in the system, does not form any azeotropes with the original components, and is completely miscible with them in all proportions. In azeotropic distillation, however, the separating agent forms one or more azeotropes with the other components in the mixture and causes two liquid phases to exist over a broad range of compositions. This immiscibility is the key to making the separation work, hence it is often referred to as heterogeneous azeotropic distillation.

Geometric methods of nonlinear analysis have proved to be very powerful tools for understanding the distillation of nonideal and azeotropic mixtures. Successful applications for homogeneous mixtures include: (1) the classification of all possible ternary mixtures (Matsuyama and Nishimura, 1977; Doherty and Caldarola, 1985), which led to methods for screening entrainers (often called solvents) for homogeneous azeotropic distillation (Foucher et al., 1991; Laroche et al., 1991); (2) the calculation of minimum reflux ratios for ideal, nonideal and azeotropic mixtures in single-feed (Julka and Doherty, 1990a; Knight and Doherty, 1986; Koehler et al., 1991) and double-feed columns (Levy and Doherty, 1986a; Knight, 1986); (3) the calculation of tangent-pinch-determined minimum reflux ratios (Levy and Doherty, 1986b; Fidkowski et al., 1991); (4) the noniterative determination of the number of theoretical trays and optimal feed plate location in multicomponent single-feed columns (Julka and Doherty, 1993); (5) the calculation of minimum flows for nonsharp splits (Julka and Doherty, 1990b); (6) the prediction of the nonintuitive order of the distillate cuts in batch distillation (Bernot et al., 1990); and (7) identification of separation regions for the distillation of nonideal ternary mixtures (Wahnschafft et al., 1992; Stichlmair and Herguijuela, 1992).

Geometric-based methods are used here to explain some key features of ternary double-feed extractive distillation columns separating minimum-boiling binary azeotropes with high-boiling entrainers or solvents—the most common industrial application of homogeneous azeotropic distillation. The much rarer separation of a maximum-boiling binary azeotrope with a low-boiling entrainer was discussed by Knapp (1991). Three major topics are covered: (1) maximum reflux ratios, (2) min-

Present address of J. P. Knapp: E. I. du Pont de Nemours & Co., P.O. Box 6090, Newark, DE 19714.

imum entrainer flows, and (3) determining which pure component can be recovered as a distillate. These three subjects have significant implications for entrainer screening, sequence synthesis and design, and operation and control. It is also important to note that all three of these can be determined for a desired separation before beginning any column design calculations.

Extractive distillations can be performed *only* in double-feed columns, and every extractive distillation exhibits a maximum reflux above which it is no longer possible to achieve the desired separation. This value depends strongly on the amount of entrainer present. Fortunately, in the range of economical entrainer flows, maximum reflux results from a specific geometrical construct that can be easily calculated.

It is easy to argue that there must exist a minimum entrainer flow in extractive distillation. The isobaric distillation of a binary homogeneous azeotrope into pure-component products is impossible without the addition of an entrainer. The presence of one molecule of entrainer per mole of feed is clearly not sufficient to make the separation feasible, yet extractive distillation with a "reasonable" amount of entrainer is a commonly used separation technique. Logically there must exist a minimum amount of entrainer between these two bounds that just makes the separation possible. We will show that this minimum entrainer flow corresponds to a simple geometric form and that it is related to the maximum reflux ratio.

Different entrainers can cause different components to be recovered overhead in extractive distillation. For example, when water is used as the entrainer to separate acetone and methanol, acetone is the distillate product. However, when methyl ethyl ketone (MEK) is used as the entrainer to separate an identical acetone-methanol mixture, it is impossible to recover acetone as the overhead product. Instead, the higher boiling MEK-methanol azeotrope becomes the distillate. This seemingly unusual behavior, whereby an intermediate-boiling azeotrope or pure component distills overhead instead of the low-boiling component, has actually been known for many years and has been observed for a number of mixtures, though it is seldom discussed in the recent literature and is therefore perhaps no longer widely known (the recent article by Laroche et al., 1991, is a notable exception). The geometrical insights derived from our analysis also explains why the intermediate-boiling pure component is sometimes the product and why, for a given entrainer, only one of the two nonentrainer constituents can be recovered as the pure product in an extractive distillation column, despite the apparent symmetry of the extractive distillation residue curve map.

Finite-Difference Model

The backbone of the geometrical methods is an analysis of the fixed points of the finite difference equations describing the various column sections. Fixed points occur where the composition does not vary from stage to stage. When these points occur on the column composition profile, they are normally referred to as pinches. Although all the phenomena to be discussed were originally identified using a model with heat effects included, we shall assume negligible heat effects (constant molar overflow) everywhere except in the sequence designs at the end of this article because the inclusion of heat effects gives rise to implicit maps that complicate the analysis with no additional insight. A consequence of the constant molar overflow (CMO) assumption is that the liquid and vapor molar flow rates are constant in each column section, but can vary between sections. We also assume (1) theoretical stages (vapor-liquid equilibrium is achieved on each tray), (2) no pressure drop across the column, and, strictly for convenience, (3) both the distillate and bottoms products are saturated liquids. These are identical to the assumptions made by Julka and Doherty (1990a) and Fidkowski et al. (1991).

The finite-difference equations describing the rectifying and stripping sections of a double-feed column are the same as those given by Julka and Doherty (1990a) for a single-feed column.

Rectifying Section:

$$\underline{y}^r_{m+1} = \frac{r}{r+1}\,\underline{x}^r_m + \frac{1}{r+1}\,\underline{x}_D \quad (m = 0, 1, 2, \ldots) \tag{1a}$$

$$\underline{x}^r_0 = \underline{x}_D \tag{1b}$$

$$r = \frac{L_T}{D} \tag{2}$$

$$r+1 = \frac{V_T}{D} \tag{3}$$

Stripping Section:

$$\underline{x}^s_{n+1} = \frac{s}{s+1}\,\underline{y}^s_n + \frac{1}{s+1}\,\underline{x}_B \quad (n = 0, 1, 2, \ldots) \tag{4a}$$

$$\underline{x}^s_0 = \underline{x}_B \tag{4b}$$

$$s = \frac{V_B}{B} \tag{5}$$

$$s+1 = \frac{L_B}{B} \tag{6}$$

where $\underline{y}_n$ is in equilibrium with $\underline{x}_n$ and the reboiler and condenser are counted as stage zero in their respective sections, as shown in Figure 1.

The middle-section equations can be described in terms of either the reflux ratio or the reboil ratio by counting trays up from the stripping section or down from the rectifying section, respectively (Knight, 1986). For direct splits, which includes the extractive distillation of minimum-boiling azeotropes, it is more natural to write the middle-section equations in terms of the reflux ratio. (The natural form of the middle-section equations for indirect splits, including extractive distillation of maximum-boiling azeotropes, was discussed by Knapp, 1991.) The middle-section finite-difference equation, also called the middle-section map, is derived in Appendix A.

Middle Section:

$$\underline{x}^m_{k+1} = \left[\frac{r+1+(q_U-1)h(Fr,\,\underline{w})}{r+q_U h(Fr,\,\underline{w})}\right]\underline{y}^m_k + \left[\frac{h(Fr,\,\underline{w})\underline{x}_{F_U} - \underline{x}_D}{r+q_U h(Fr,\,\underline{w})}\right] \quad (k = 0, 1, 2, \ldots) \tag{7a}$$

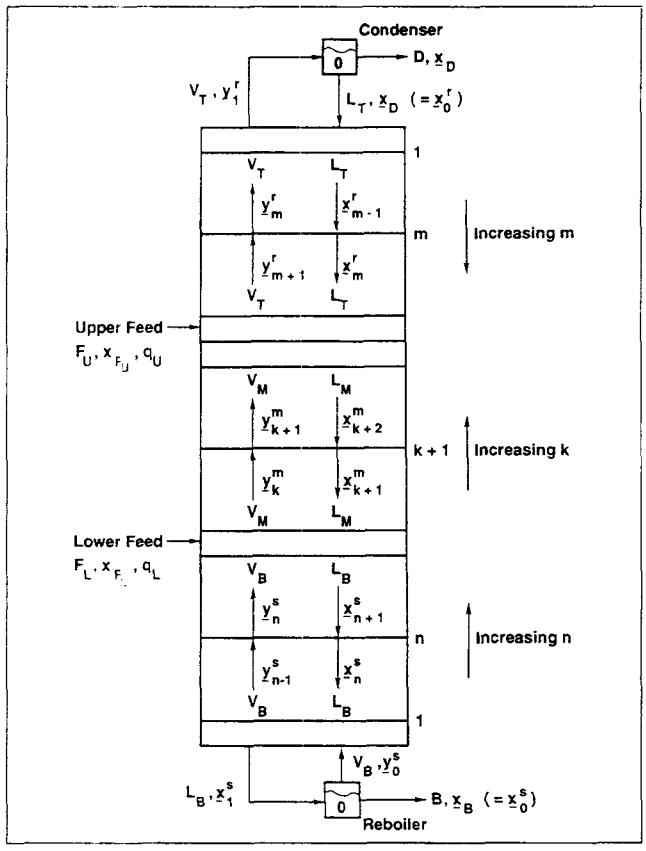

Figure 1. Double-feed distillation column.

where the function $h(Fr, \underline{w})$ is defined by Eq. A9 and depends only on the feed ratio (Fr) and the feed, distillate, and bottom compositions. Since the middle-section trays are counted upward from the lower feed tray in this problem formulation, the initial condition for the middle section is the composition on the last tray, N, of the stripping section:

$$\underline{x}_0^m = \underline{x}_N^s \tag{7b}$$

The reflux and reboil ratios are related by:

$$s = (r+1)\frac{D}{B} + \frac{F_L}{B}\left[Fr(q_U - 1) + (q_L - 1)\right] \tag{8}$$

Equations A7 and A8 can be incorporated into Eq. 8 to eliminate the dependence on flow rates. When the feed ratio is set to zero (a single-feed column), Eq. 8 correctly reduces to the relationship between r and s for single-feed columns given by Julka and Doherty (1990a).

Just like in single-feed columns, the behavior of the liquid-phase composition profiles in each section of a double-feed column is governed by the location of the fixed points of the corresponding column-section equations. The fixed points, $\hat{\underline{x}}$, are those points where the composition does not change from stage to stage ($\underline{x}_n \to \underline{x}_{n+1} \to \hat{\underline{x}}$):

Rectifying Section:

$$\frac{r}{r+1}\hat{\underline{x}}^r - \hat{\underline{y}}^r + \frac{1}{r+1}\underline{x}_D = 0 \tag{9}$$

Stripping Section:

$$\frac{s}{s+1}\hat{\underline{y}}^s - \hat{\underline{x}}^s + \frac{1}{s+1}\underline{x}_B = 0 \tag{10}$$

Middle Section:

$$\left[\frac{r+1+(q_U-1)h(Fr, \underline{w})}{r+q_U h(Fr, \underline{w})}\right]\hat{\underline{y}}^m - \hat{\underline{x}}^m + \left[\frac{h(Fr, \underline{w})\underline{x}_{F_L} - \underline{x}_D}{r+q_U h(Fr, \underline{w})}\right] = 0 \tag{11}$$

In the limiting case of total reflux ($r \to \infty$) [total reboil ($s \to \infty$) for Eq. 10], Eqs. 9 to 11 all reduce to:

$$\hat{\underline{x}} = \hat{\underline{y}} \tag{12}$$

(For the middle section, this reduction is easier to see by letting the internal flow rates become infinite in the fixed-point version of Eq. A14.) Therefore, at total reflux (reboil), the fixed points inside the composition state space for all three column sections lie at the pure-component vertices and azeotropic compositions of the composition simplex. Furthermore, Julka (1993) proved that all the fixed points on the boundary and interior region of the multicomponent simplex must be stable nodes, unstable nodes, or saddles, and that oscillatory solutions, Hopf bifurcations, and period-doubling bifurcations are not possible. These observations are important because they make it possible to track *all* fixed-point branches lying inside the composition state space (Fidkowski et al., 1991; Julka and Doherty, 1993) and to qualitatively predict the shape and location of the liquid-phase column profiles, knowing only the residue-curve map, the feed composition, and the desired distillate and bottoms compositions.

Geometry of Double-Feed Distillation Column Profiles

To provide a setting for the methods developed later we first describe the reasons for tracking branches of fixed points. We show that this procedure provides all the necessary information required for design without having to solve the stage-to-stage balances.

The stability of the fixed points in each column section at total reflux (reboil) can be predicted from a residue-curve map of the mixture (that is, the infinite reflux composition profiles) and some simple temperature-based arguments. (Of course, the stability of the various fixed points can only rigorously be determined by calculating eigenvalues. See Julka and Doherty, 1990a, for details.) Temperature always increases along simple-distillation residue curves (Doherty and Perkins, 1978). The rectifying-section profile starts at the distillate composition leaving the condenser, typically the lowest temperature in the column, and proceeds down the column in the direction of increasing temperature. Therefore, the stability of fixed points in the rectifying section at $r \to \infty$ will be the same as the stability of singular points in the residue-curve map. The stripping-section profile starts with the bottoms composition leaving the reboiler, typically the highest temperature in the column, and

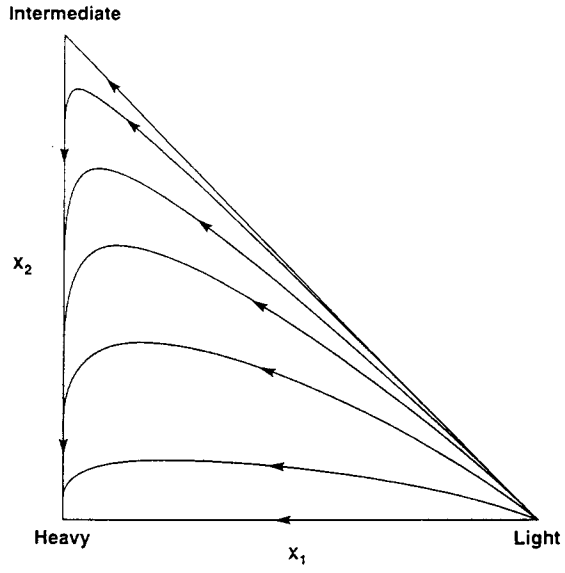

Figure 2. Generic residue-curve map for a nonazeotropic mixture shown in the standard orientation.

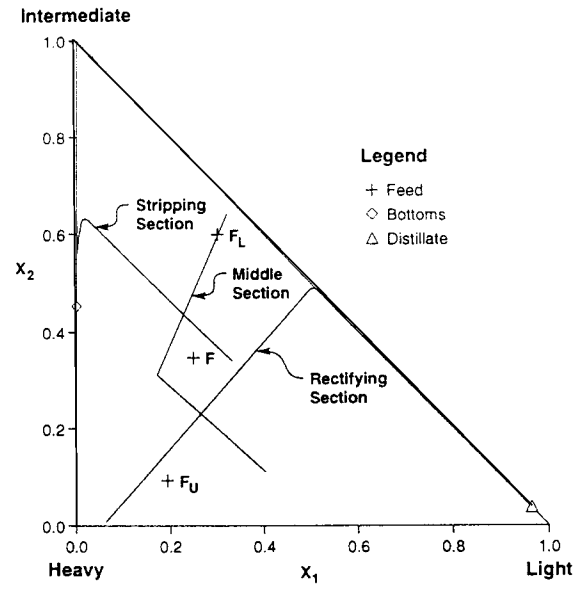

Figure 3. Typical column profiles for a nonazeotropic mixture in a double-feed column.

proceeds up the column in the direction of decreasing temperature. Therefore, at $s \to \infty$, the stability of stripping-section fixed points will be opposite to the stability of singular points in the residue-curve map. In other words, stable nodes on the residue-curve map correspond to unstable nodes in the stripping section, unstable nodes in the residue-curve map correspond to stable nodes in the stripping section, and saddles on the residue-curve map correspond to saddles in the stripping section, but with opposite orientation. The middle-section map, Eq. 7, is written in terms of the reflux ratio, and stages are counted up from the lower feed tray, that is, in the direction of decreasing temperature, just like the stripping-section profile. Therefore, the stability of fixed points in the middle-section map at $r \to \infty$ is the same as the stability of stripping-section fixed points at $s \to \infty$. The stability (but not the location) of each fixed point in each column section will remain unchanged at lower values of the reflux (reboil) ratio unless a point of local or global bifurcation is encountered.

Knowing only the residue-curve map for a mixture, the general shape of the column profiles can often be estimated using these temperature-based fixed-point stability arguments. The actual locations of the fixed points at the specified reflux (reboil) ratio are necessary to get a more detailed picture. To see the geometric similarity of all direct and indirect splits, the residue-curve maps and column profiles should be drawn in a *standard orientation*. The standard orientation that we select for ternary mixtures places the column product (usually the light component for direct splits and the heavy component for indirect splits) at the lower righthand corner of the composition triangle, the nonproduct (typically the intermediate-boiling pure component) at the top vertex, and the entrainer or heavy component (light component for indirect splits) at the origin. For example, consider the residue-curve map for a nonazeotropic mixture shown in Figure 2. For a sharp direct split, the distillate is located near the light component vertex close to the $x_{\text{heavy}} = 0$ edge of the triangle. The rectifying profile moves up along this edge (near the unstable separatrix of the rectifying saddle) until it reaches the location of the rectifying-section saddle that originates at the intermediate-boiling-component vertex when $r \to \infty$. The rectifying profile then turns and moves across the composition triangle, roughly following the stable separatrix of the rectifying saddle, until it ends at the stable node originating at the heavy-component vertex (Figure 3). (The stable and unstable separatrices of a saddle point are the four special trajectories that divide the four regions of hyperbolic trajectories about the saddle point.) The bottom product composition is located near the $x_{\text{light}} = 0$ edge. (The exact location of $\underline{x}_B$ is determined by a mass balance around the column.) The stripping-section profile, which generally moves in the direction of decreasing temperature, originates at $\underline{x}_B$ and then moves up along the $x_{\text{light}} = 0$ edge toward the location of the stripping-section saddle originating from the intermediate-boiling-component vertex. The stripping profile then turns and moves across the triangle until it ends at the stable node coming from the light-component vertex (Figure 3). Thus, the rectifying and stripping sections of a double-feed column exhibit the same familiar shapes as in single-feed columns. (See the figures in Levy et al., 1985; Levy and Doherty, 1986a; Julka and Doherty, 1990a, 1993, but beware that some of these figures are not drawn in the standard orientation.) Also like single-feed columns, the sharpness of the column profiles (their closeness to the stable and unstable separatrices) is affected by varying the amounts of heavy component in the distillate and light component in the bottoms.

The shape of the middle-section profile is determined as follows. Two stable and two unstable separatrices (manifolds) are associated with every saddle fixed point. As the reflux ratio is decreased from $r = \infty$, the middle-section saddle (located at the intermediate-boiling-component vertex at total reflux) moves inside the composition triangle, bringing its separatrices with it. (The orientation of the separatrices can rotate as the reflux decreases.) Thus, at finite reflux the middle-section saddle divides the composition state space into four regions (Figure 4). At total reflux region A corresponds to the entire com-

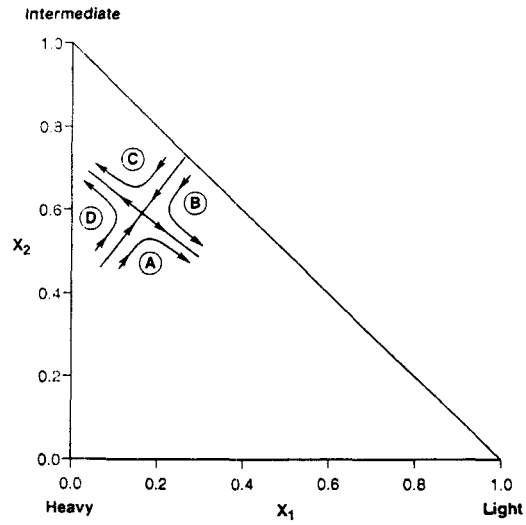

Figure 4. Middle-section saddle fixed point for a direct split at finite reflux.

Note how the separatrices divide the composition space into four regions.

position triangle: at $r = \infty$, the separatrices marking the boundary of region A are the two sides of the composition triangle. The middle-section profile can lie in any of these four regions depending on the location of the initial condition for the middle section. (The stripping and rectifying sections cannot exhibit this behavior because there is only one possible initial condition for each of these sections, $\underline{x}_B$ and $\underline{x}_D$, respectively.) For example, Figure 4a in Levy and Doherty (1986a) shows the middle profile switching from region D to region A as the initial condition is changed from the liquid composition on tray 8 of the stripping section to the liquid composition on tray 9. Although it is possible for the middle profile to lie in any of these four regions, only regions A and B give rise to feasible column designs (see Figures 4a, 5a and 8 of Levy and Doherty, 1986a).

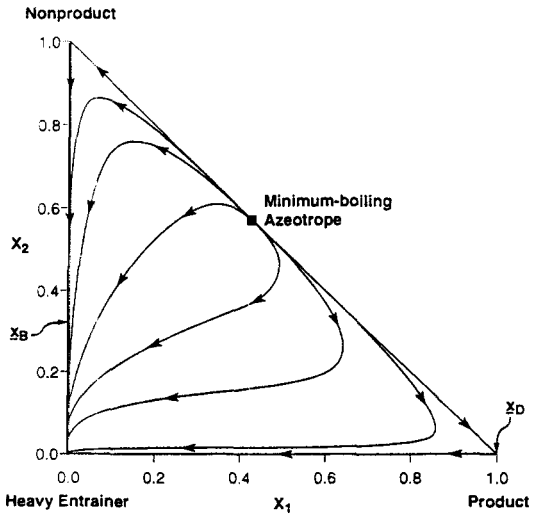

Figure 5. Residue-curve map for the extractive distillation of a minimum-boiling azeotrope (shown in the standard orientation).

Typical distillate and bottoms compositions are also indicated.

Figure 3 shows the middle-section profile lying in region B. The two feasible regions, A and B, share the common feature that the stable separatrix between them is connected to the middle-section stable node originating at the light-component vertex. Therefore, knowledge of the location of the middle-section saddle and stable node, plus the initial condition for this section, is sufficient to completely determine the qualitative shape of the middle-section profile without having to solve the stage-to-stage balances.

Geometry of Ternary Extractive Distillation Column Profiles

The geometry of extractive distillation column profiles is also determined from a combined analysis of the residue curve map and the column fixed points. There is only one residue-curve map that represents the extractive distillation of a minimum-boiling binary azeotrope, shown in the standard orientation in Figure 5. To be as general as possible, the component recovered as the distillate product is identified as the "product" component and the other nonentrainer component is referred to as the "nonproduct." Although the lowest-boiling component is usually the one recovered as the distillate, this is not always the case. Note that the azeotrope is an unstable node, the entrainer is a stable node, and the two pure components of the original binary mixture are saddles on the residue-curve map. The same temperature-based arguments discussed in the previous section for predicting the stability of the fixed points in the various column sections apply here also.

For extractive distillation, a properly chosen distillate composition lies near the "product" vertex close to the base of the triangle. (If the distillate were placed near the "product" vertex but close to the "product"–"nonproduct" edge of the triangle, the rectifying section would needlessly require a large number of trays merely to move past the saddle at the "product" vertex and reach the position of a properly chosen distillate. This is only justifiable if there is a process constraint on the amount of entrainer allowed to leave in the distillate.) The rectifying-section profile simply moves along the base of the composition triangle and ends at the rectifying-section stable node which comes from the entrainer vertex. The bottoms composition is located near the vertical edge of the triangle with its exact position determined by mass balance. The stripping profile moves upward, close to the $x_l = 0$ edge, until it approaches the location of the stripping-section saddle originating at the "nonproduct" vertex. Near this saddle the profile turns and, roughly following the saddle's stable separatrix, moves across the composition triangle until it ends at the stripping-section stable node which originates at the azeotrope.

An important point can be made from this knowledge of the general shapes of the rectifying and stripping profiles in extractive distillations. The rectifying profile always starts from a distillate composition near the "product" vertex and moves along the base of the composition triangle, and the stripping profile must end at the stable node originating at the azeotrope. Thus, the only way that an extractive distillation could be achieved in a single-feed column is if the stripping-section stable-node branch (the locus of stripping-section stable nodes calculated over a range of reboil ratios) were to reach the base of the composition triangle at some reboil ratio. Consequently, extractive distillations can *never* take place in a single-feed

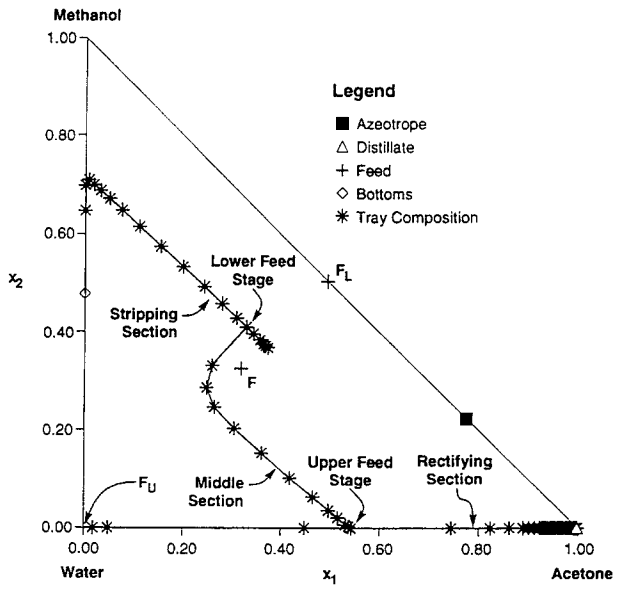

Figure 6. Extractive distillation column profiles at a feed ratio of 0.55 for the acetone-methanol-water separation described in Knapp and Doherty (1990).

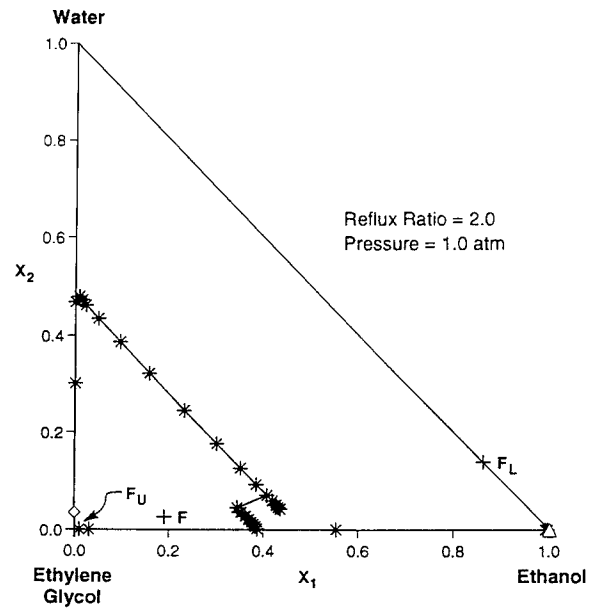

Figure 7. Extractive distillation column profiles at a feed ratio of 3.5 for the ethanol-water-ethylene glycol separation in Figure 11 of Levy and Doherty (1986a).

column at total reflux (reboil) because the stripping section's stable node is located at the azeotrope. In fact, after studying a number of extractive distillations over a wide range of feed ratios, there is no evidence that the stripping-section stable node can ever cross the rectifying profile (except possibly with an infinite amount of entrainer). Therefore, extractive distillations require double-feed columns where the middle-section profile acts as a bridge between the nonintersecting rectifying and stripping profiles. This agrees with the conventional description of extractive distillation, which states that the heavy entrainer must be fed near the top of the column so that it is present throughout most of the column at a high enough concentration to make the separation possible by sufficiently modifying the relative volatilities of the key components.

The geometric behavior of the middle-section profile in extractive distillation is governed by the presence of two saddle points. Key questions include: (1) which saddle controls the middle-section profile's behavior, (2) is it always the same saddle, and (3) if not, what determines the switching of control from one saddle to the other? The simple arguments used above cannot answer these questions. These arguments, however, can be used to make one extremely significant point about the middle-section profile of every extractive distillation. At total reflux (reboil) the stable node for the middle section lies at the minimum-boiling azeotrope. The middle profile starts at some tray composition in the stripping section (at some point along the edge of the triangle supported by the bottoms composition, the "nonproduct" vertex and the azeotrope) and *must* end at this stable node; yet, a feasible extractive column requires the middle-section profile to intersect the rectifying profile, which always lies along the base of the triangle. Therefore, extractive distillations can never be feasible at total reflux (reboil). Of course, extractive distillation at finite reflux ratios is known to be feasible and is commonly used in industry. Thus, there must always be some value of the reflux above which the separation is suddenly no longer possible, that is, *every extractive distillation must exhibit a maximum feasible reflux.* This is true at all entrainer flows above the minimum.

Figures 6, 7, 8 and 9 show feasible extractive distillation column profiles for four mixtures. The two feed stages and the three column sections are explicitly identified on Figure 6. The other figures should be interpreted in a similar way. Note that each corresponding column section has a similar shape in each of the four examples and that these shapes agree with the

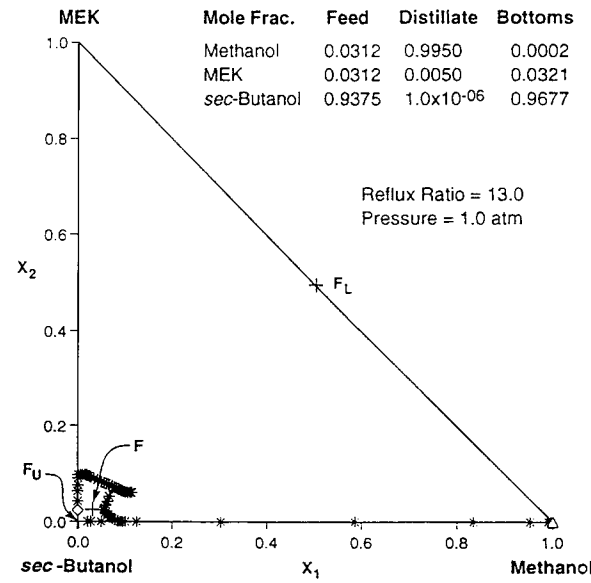

Figure 8. Extractive distillation column profiles at a feed ratio of 15 for the methanol-MEK-*sec*-butanol mixture.

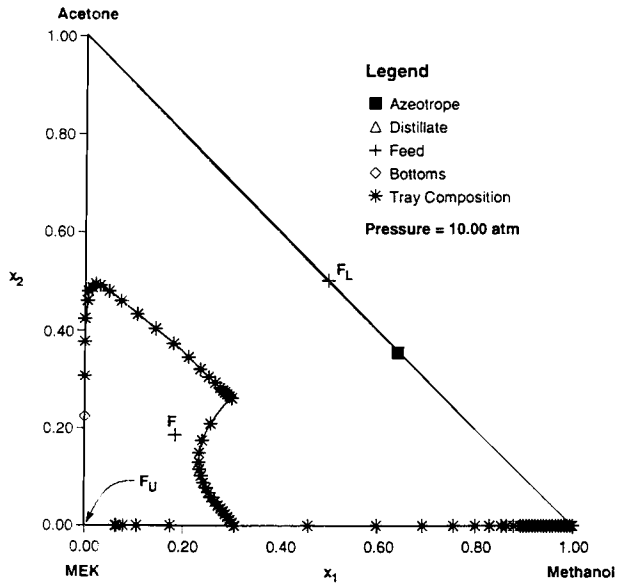

Figure 9. Column profile for the first column of the methanol-acetone-MEK pressure-swing distillation sequence.

arguments outlined above. The models used to calculate these profiles are given by Knapp (1991).

Fixed-Point Analysis of the Middle-Section Map

The fixed points of each column section completely define the behavior of that section's profile. Since the behavior of rectifying and stripping profiles in double-feed columns is completely understood in terms of the results for single-feed columns, only the fixed points of the middle section need to be studied.

To avoid ambiguity, the fixed points of the middle section will always be identified by the following labeling scheme:

SN = stable node originating at the azeotrope
S1 = saddle originating at the "product" vertex
S2 = saddle originating at the "nonproduct" vertex
UN = unstable node originating at the entrainer vertex
SN^- = stable node originating outside the composition simplex
UN^- = unstable node originating outside the composition simplex

The fixed points lying outside the composition triangle have no physical meaning. However, the middle section profile which lies inside the physically meaningful region behaves as if fixed points exist outside the composition triangle; by allowing for their mathematical existence a consistent description of the behavior of the middle-section map can be developed. It should be emphasized that none of the methods, which will be developed for determining minimum entrainer flows, maximum reflux ratios and which component becomes the pure product, require calculations outside of the composition simplex.

As an introduction to the behavior of the middle-section map, consider the phase planes in Figures 10 and 11 for the acetone-methanol-water separation from Knapp and Doherty (1990). Figure 10 shows how the structure of the solution space for the middle-section map changes as the maximum reflux ratio (r_{max}) is crossed. Above r_{max} (Figure 10a), the phase plane is as expected from the infinite reflux analysis of the previous

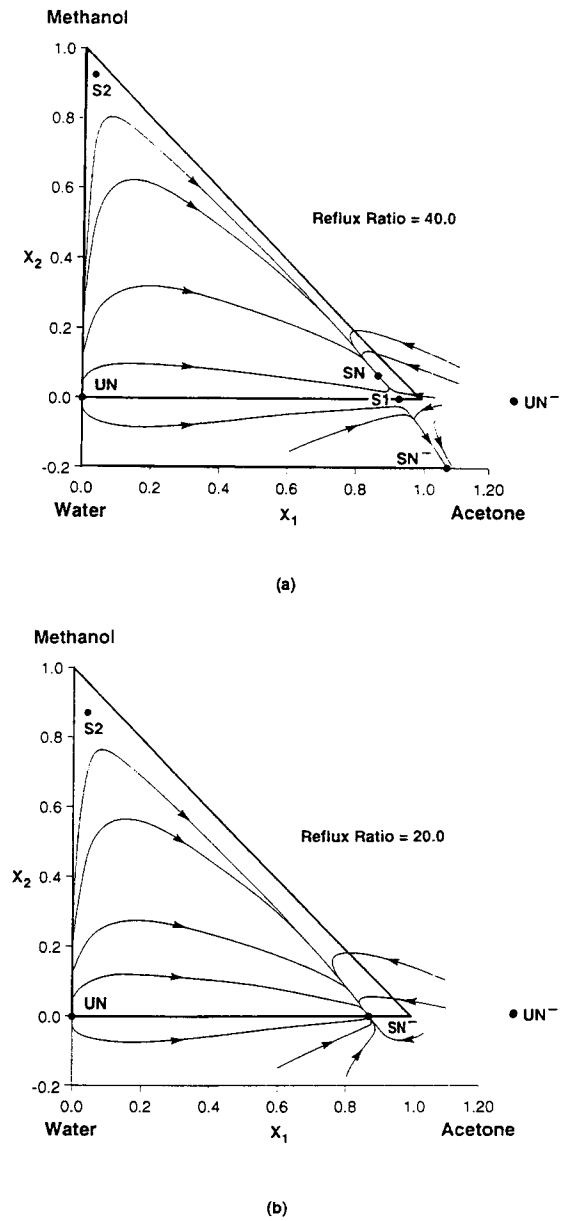

Figure 10. Middle-section phase planes for the acetone-methanol-water separation at a feed ratio of 0.55: (a) above and (b) below maximum reflux.

section. There is an unstable node (*UN*) coming from the water vertex, a saddle (*S2*) coming from the methanol (nonproduct) vertex, a stable node (*SN*) coming from the acetone-methanol azeotrope, and a saddle (*S1*) coming from the acetone (product) vertex. Because four separatrices are associated with every saddle fixed point in two dimensions (Figure 4) and a fixed point lies at the end of each separatrix, both *S1* and *S2* should be connected to additional fixed points. The four fixed points connected to *S1* by its separatrices are the *UN* and *SN* mentioned above, and the stable (SN^-) and unstable (UN^-) nodes lying outside the composition triangle. Above r_{max}, the middle-section column profile ends at *SN* and is prevented from intersecting the rectifying profile by the separatrix connecting *UN* to *S1*. Contrast this with the phase plane below r_{max} in Figure 10b. Note that the fixed points *SN* and *S1* have dis-

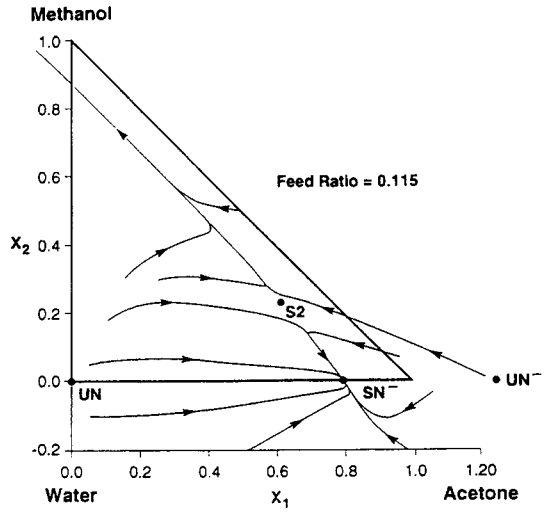

(a)

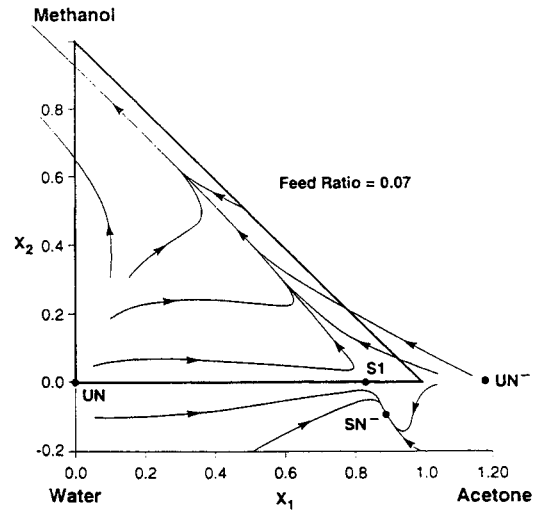

(b)

Figure 11. Middle-section phase planes for the acetone-methanol-water separation at a reflux ratio of 3.0: (a) above and (b) below the minimum entrainer flow.

appeared and that SN^- now lies just outside the composition triangle. Because SN no longer exists to attract trajectories and because the UN-$S1$ separatrix disappears along with $S1$, the middle-section profile can now intersect the rectifying profile.

Figure 11 shows how the structure of the solution space for the middle-section map differs above and below the minimum feed ratio (Fr_{min}). Above Fr_{min} but below r_{max} (Figure 11a), the phase plane is globally the same as that shown in Figure 10b; only the positions of the fixed points have changed, most noticeably $S2$. Also note the stable separatrix leading away from $S2$ in the direction of the methanol vertex. This indicates that there is another attracting fixed point outside the composition state space in that general direction which provides the required fourth fixed-point connection to the saddle $S2$. Although it cannot be seen in the figure, this same additional attracting fixed point exists at the conditions of Figure 10b. Below Fr_{min} (Figure 11b), fixed point $S2$ does not exist, but saddle $S1$ does. The presence of the separatrix from UN to $S1$ again prevents the middle-section profile from crossing the rectifying profile and reaching SN^- (a feasible column design is impossible). Instead, the middle profile moves in the opposite direction toward the attracting fixed point lying outside the triangle in the direction of the methanol vertex.

The change in the number of fixed points in the middle-section map between the conditions shown in parts a and b of Figures 10 and 11 indicates that bifurcations have occurred. While phase planes show all the features of the map, they do not provide an efficient method for locating the parameter values at which these bifurcations occur. A more powerful technique is to study the behavior of the middle-section fixed-point branches. Such branches have already proved to be invaluable for calculating minimum flows (Julka and Doherty, 1990a), tangent pinches (Fidkowski et al., 1991), and theoretical stages (Julka and Doherty, 1993) in nonideal and azeotropic distillations.

Fixed-point branches are the locus of fixed points as a function of the reflux (or reboil) ratio for specified values of the remaining parameters. These branches are continuous curves in C-dimensional ($\underline{x}$, r) space (three-dimensional space here) which originate from the pure components and azeotropes at infinite reflux and which can be robustly tracked using an arc-length or pseudo-arc-length continuation method such as AUTO (Doedel, 1986). The stability characteristics of each branch can be assessed from the eigenvalues of the Jacobian of the middle-section map, as discussed by Knapp (1991), Doedel (1986), Julka and Doherty (1990a), and Julka (1992). By convention, a stable (stable node) fixed-point branch is represented by a solid line, and an unstable (either a saddle or an unstable node) fixed-point branch is represented by a dashed line. Fixed-point branches are viewed best by projection onto the (x_1, x_2), (x_1, r) or (x_2, r) plane. Each point along a fixed-point branch in the (x_1, x_2) projection corresponds to a different value of the reflux ratio. Since a phase plane can be qualitatively sketched knowing only the location of the fixed points, the (x_1, x_2) projection of the fixed-point branches summarizes the information contained in a series of phase planes at different reflux ratios. There is no guarantee that all projections of the fixed-point branches will show all the special features of the map. Indeed, there are certain special conditions under which they clearly will not. For example, if a fixed-point branch lies entirely in a plane parallel to the x_1 axis (x_2 = constant), the branch would be fully visible in the (x_1, r) projection, but appear only as a line in the (x_2, r) projection. Fidkowski et al. (1991) provide a method for determining a set of sufficient conditions to ensure that the different projections all exhibit the same special features at the same parameter values. We have never encountered a case where the (x_2, r) projection showed features not present in the (x_1, r) projection. Therefore, throughout the remainder of this article, only the (x_1, r) and (x_1, x_2) projections will be used.

Maximum Reflux Ratios

Although it is possible to follow the fixed-point branches for any combination of the six fixed points ($S1$, $S2$, UN, UN^-, SN^-, and SN) shown in the phase planes of Figures 10 and

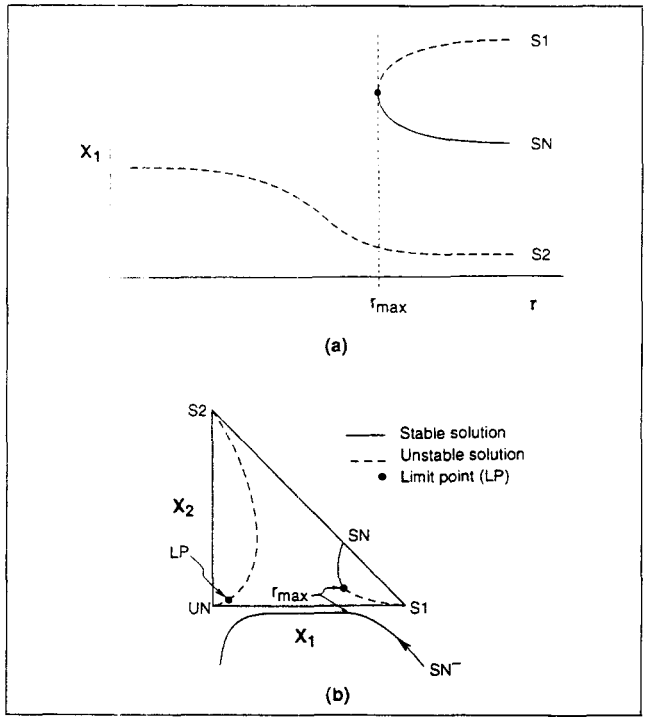

Figure 12. Fixed-point branches showing r_{max} behavior at fixed $Fr > Fr_{min}$: (a) (x_1, r) projection of the *S1*, *SN*, and *S2* fixed-point branches; (b) (x_1, x_2) projection showing all pertinent fixed points.

Note the limit points between *S1* & *SN* and *S2* & *UN*.

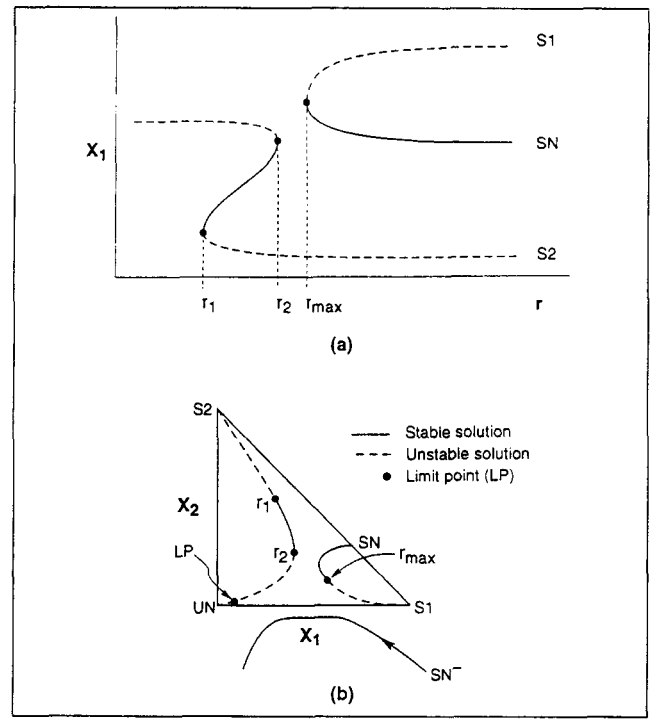

Figure 13. Fixed-point branches showing r_{max} behavior at fixed $Fr \simeq Fr_{min}$: (a) (x_1, r) projection; (b) (x_1, x_2) projection showing all pertinent fixed points.

Note the hysteresis in the *S2* branch.

11, the *S1*, *S2*, and *SN* fixed-point branches contain all the information necessary to determine both the maximum reflux ratio (r_{max}) and the minimum entrainer flow (Fr_{min}).

From the (x_1, r) projection of the fixed-point branches (Figure 12a), it is easy to see that r_{max} corresponds to a limit point (also commonly called a turning point or saddle-node bifurcation) between *S1* and *SN*. This is the normal r_{max} behavior, which always occurs at feed ratios in the neighborhood of Fr_{min} and usually persists over and beyond the range of likely operating feed ratios. However, at sufficiently large va.ues of Fr, maximum reflux no longer corresponds to a limit point between *S1* and *SN*. This case is treated in Appendix B.

From infinite reflux down to the maximum reflux, the middle-section trajectories are always attracted to the *SN* branch; because trajectories cannot cross separatrices, the separatrix between *UN* and *S1* prevents the middle-section profile from intersecting the rectifying profile, which lies along the base of the composition triangle (Figures 10a and 12b). These two features cause maximum reflux to exist. At r_{max} (Figures 12a and 12b), the *S1* and *SN* branches coalesce and eliminate each other. (A phase plane would show a nonelementary saddle-node fixed point as in Figure 5b of Levy and Doherty, 1986b). At the same time, the SN^- branch, which originated far outside the composition triangle, has moved and now lies just outside the base of the triangle. Consequently, for reflux ratios above the minimum but below the maximum, the SN^- branch is now accessible and becomes the branch of attracting fixed points. The middle profile can now intersect the rectifying profile because neither *S1*, *SN* nor the *UN*-*S1* separatrix exists. Figure 10b shows a typical phase plane below r_{max} for $Fr > Fr_{min}$. Thus, the middle-section profile for a feasible extractive distillation column ($r_{min} < r < r_{max}$) will start from the liquid-phase composition of some stripping-section tray, "bounce" off of the *S2* saddle, cross the rectifying profile, and end just outside the triangle at SN^-. This is precisely the geometry exhibited by the extractive distillation column profiles in Figures 6, 7, 8 and 9, and also demonstrates the conceptual importance of fixed points which lie outside of the composition state space.

Figure 12b also shows a limit point between *S2* and *UN*. This limit point always exists; in all the examples studied, it occurs at reflux ratios well below r_{min}. Because the *S2*-*UN* limit point typically occurs at low reflux, it normally will not be visible on the same (x_1, r) plot showing the *S1*-*SN* limit point. The methanol-MEK-*sec*-butanol example is one exception. Also at very small reflux ratios, the SN^- branch turns and moves away from the composition triangle, as shown in Figures 12b–15b. One point of purely theoretical curiosity is that there are no more middle-section fixed points *inside* the feasible state space at reflux ratios below that at which the *S2*-*UN* limit point occurs.

The value of the maximum reflux ratio depends strongly on the feed ratio, in such a way that r_{max} increases as Fr increases. As the feed ratio decreases, the *S2* branch and the combined *S1* and *SN* branches start to move toward each other. (Compare Figure 12b with Figure 13b.) In the neighborhood of Fr_{min}, a new phenomenon appears. One of the saddle branches starts to exhibit a hysteresis loop (Figure 13). Although the *S1* branch sometimes exhibits hysteresis behavior, most of the examples studied have the hysteresis loop in the *S2* fixed-point branch.

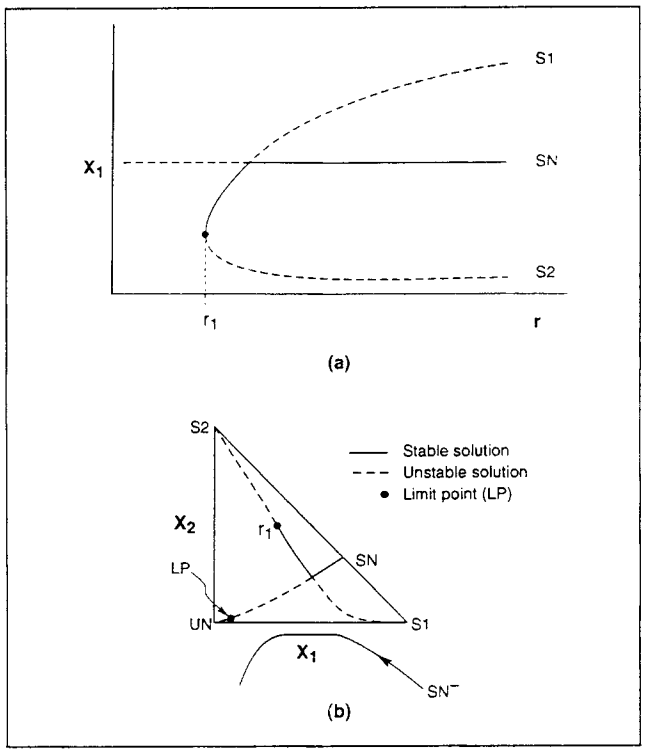

Figure 14. Fixed-point branches at Fr_{min}: (a) (x_1, r) projection showing a perturbed pitchfork bifurcation; (b) (x_1, x_2) projection showing the *S1*, *SN* and *S2* branches meeting at a single point.

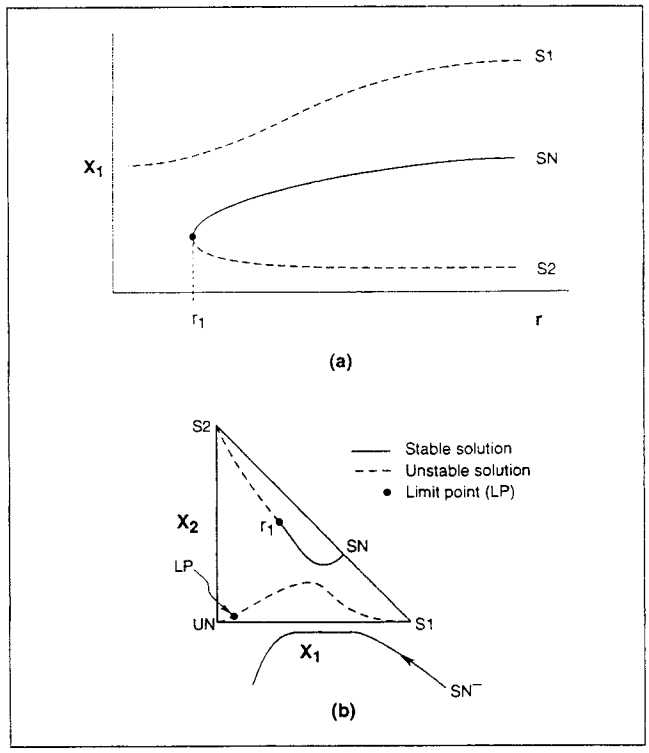

Figure 15. Fixed-point branches at fixed $Fr < Fr_{min}$: (a) (x_1, r) projection of the *S1*, *SN*, and *S2* branches; (b) (x_1, x_2) projection showing all pertinent fixed point branches.

Note that now *S2* & *SN* and *S1* & *UN* meet at limit points.

Sometimes this hysteresis exists over such a small range of feed ratios that it is almost undetectable, while in other cases it can persist at feed ratios as large as 1.7 Fr_{min}. (Hysteresis can also occur in other fixed-point branches. For example, the SN^- branch for the acetone-methanol-water separation exhibits hysteresis at certain reflux ratios for $0.3 \leq Fr \leq 1.0$.)

The presence of the hysteresis loop complicates the behavior of the middle-section map. At any reflux ratio between r_1 and r_2 (see Figure 13a), there are simultaneously three fixed points on the *S2* branch and they are all observable. Although none of the phase planes in Figures 10 and 11 show this hysteresis behavior, it is possible to draw one which does. It, however, will not be apparent that it is indeed a hysteresis loop until the (x_1, r) projection of the fixed-point branch is drawn. For $r > r_2$, the middle-section behavior is identical to that described above. For $r > r_{max}$, all trajectories are attracted to *SN* and no feasible column design is possible. At $r = r_{max}$, the *S1* and *SN* branches meet at a limit point and cease to exist. For $r_2 < r < r_{max}$, all trajectories are attracted to SN^- and feasible column designs are possible. Then, at $r = r_2$, another stable node and another saddle point appear which act just like the branches *S1* and *SN* did at $r > r_{max}$: for $r_1 < r < r_2$, there is a separatrix from *UN* to this new saddle which makes the SN^- branch inaccessible. Instead, all of the middle-section trajectories are attracted to the new stable node on the *S2* branch. Thus, between r_1 and r_2, it again becomes impossible to design a feasible column. At $r = r_1$, one of the saddles and the stable node on the *S2* branch eliminate each other at a limit point. This is entirely analogous to r_{max}. Therefore, for $r_{min} < r < r_1$, the SN^- branch is once again accessible and feasible column designs are possible. In other words, r_2 acts as a second r_{min} and r_1 acts as a second r_{max}. Fortunately, from a practical point of view, this complex hysteresis behavior is easily avoided because economically optimum values for the feed ratio are sufficiently greater than Fr_{min} that this hysteresis does not occur (see the examples).

Minimum Entrainer Flows

As the feed ratio is decreased further from its value in Figure 13, the *S2* branch and the combined *S1* & *SN* branches continue to approach each other until, at a specific feed ratio, all three branches meet at a single point (Figure 14b). This corresponds to the coalescence of the limit points at r_2 and r_{max} in Figure 13 and results in the perturbed pitchfork bifurcation in Figure 14a. The feed ratio at which this perturbed pitchfork bifurcation occurs is the minimum feed ratio (Fr_{min}). Below Fr_{min}, the *SN* branch meets the *S2* branch (not the *S1* branch as before) at a limit point (Figure 15). This explains why *S2* exists in the phase plane above Fr_{min} (Figure 11a), but not in the phase plane below Fr_{min} (Figure 11b), where *S1* exists instead.

For $Fr < Fr_{min}$ and $r > r_1$ (Figure 15), the middle-section trajectories inside the composition triangle will always be attracted to the *SN* branch and be prevented from reaching the SN^- branch by the *UN*-*S1* separatrix. Below r_1, the *SN* branch ceases to exist, but the *S1* saddle and its separatrices remain. These separatrices continue to deny access to the SN^- branch, which is required for a feasible design. Instead, all the middle-section trajectories inside the physically-meaningful region move to-

ward an attracting fixed point lying outside the triangle in the general direction of the nonproduct vertex as in Figure 11b. Consequently, for any $Fr < Fr_{min}$, the middle-section profile will never be able to cross the rectifying profile and reach the SN branch, making a feasible column design impossible.

Just as SN switches from meeting $S1$ at a limit point to meeting $S2$ at a limit point as Fr_{min} is crossed, UN also switches from meeting $S2$ at a limit point at very small r to meeting $S1$ at a limit point at very small r as Fr_{min} is crossed, showing the symmetry between $Fr > Fr_{min}$ and $Fr < Fr_{min}$ which is evident by comparing Figures 12 and 15. Note that as Fr is decreased below the value in Figure 15b, the $S1$ and SN branches will continue to move farther apart.

From these last two sections it is clear that both maximum reflux and minimum entrainer flow are completely defined by the $S1$, $S2$ and SN fixed-point branches. There is no reliance on calculations outside of the physically-meaningful composition state space to determine either quantity. In fact, simply following the behavior of the SN branch as r and Fr are changed is sufficient. *If SN meets S1 at a limit point, then Fr is above Fr_{min} and the reflux at which the limit point occurs is r_{max} at this value of Fr. If SN meets S2 at a limit point, then Fr is below Fr_{min}. If S1, S2, and SN all meet at the same point (a bifurcation point), then $Fr = Fr_{min}$.*

Application of Singularity Theory

Together, Figures 12a, 13a, 14a and 15a suggest that the r_{max} and Fr_{min} phenomena correspond to different perturbations of the standard pitchfork singularity in Figure 16. Thus, singularity theory offers one potential approach to calculating r_{max} and Fr_{min}.

Singularity theory (Golubitsky and Schaeffer, 1985) classifies bifurcations by their *codimension*, that is, by the number of parameters needed in the *universal unfolding* of the bifurcation or, equivalently, the highest-order zero derivative at the singularity. The universal unfolding is essentially the simplest algebraic equation capable of exhibiting a particular type of bifurcation and all its persistent perturbations. The pitchfork is a codimension-2 bifurcation and thus has two parameters, α and β, in its universal unfolding. The unperturbed pitchfork, denoted by (o) in Figure 16, corresponds to α and β both equal to zero. For α, $\beta \neq 0$, four persistent (readily observable) perturbations are possible and are labeled (a), (b), (c) and (d) in Figure 16. The boundaries between the fundamentally different persistent perturbations are called the *transition varieties*. The pitchfork has both a *hysteresis variety* ($\mathcal{H}$) and a *bifurcation or isola variety* ($\mathcal{B}$), which are shown in (α, β) space in the bottom half of Figure 16. Any point on the hysteresis variety gives rise to a bifurcation diagram containing a hysteresis point (sometimes called a critical point) as shown as (a-b) and (c-d) in Figure 16, while any point on the bifurcation variety gives rise to a bifurcation diagram containing a bifurcation point, (a-c) and (b-d) in Figure 16. Note that the unperturbed pitchfork exists only at the intersection of the two varieties. Although the same bifurcations and transition varieties can also exist in problems with more than one state variable (e.g., extractive distillation), the theory presented in Golubitsky and Schaeffer (1985) is for scalar equations only. For problems in higher-dimensional state spaces they advocate using *Liapunov-Schmidt reduction* which is rather unwieldy in practice. A very

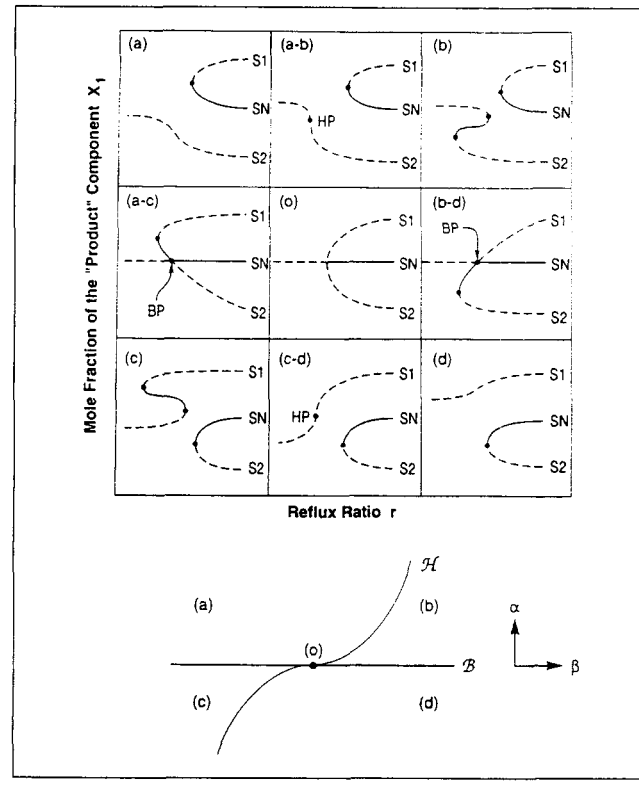

Figure 16. Bifurcation diagrams of the various perturbations of the pitchfork singularity (top), and the bifurcation ($\mathcal{B}$) and hysteresis ($\mathcal{H}$) varieties in the parameter space of the universal unfolding (bottom).

Hysteresis points are represented by *HP*, bifurcation points by *BP*.

readable and helpful account of singularity theory in the context of reaction engineering is given by Sheintuch and Luss (1983).

By comparing Figure 14a with the figures in Figure 16, it is obvious that Fr_{min} corresponds to lying on the bifurcation variety ($\mathcal{B}$). Consequently, a method for calculating the location of $\mathcal{B}$ in terms of the model parameters for a multidimensional problem would enable Fr_{min} to be found. The Liapunov-Schmidt reduction approach is not practical for our application. Fortunately, in an earlier article, Golubitsky and Schaeffer (1979) present general, n-dimensional formulas for the transition varieties. The bifurcation variety of an n-dimensional system of equations $\underline{f}(\underline{u}, \lambda, \underline{\alpha}) = \underline{0}$ is defined as:

$$\mathcal{B} = \{\underline{\alpha} \mid \exists (\underline{u}, \lambda) \text{ with } \underline{f}(\underline{u}, \lambda, \underline{\alpha}) = \underline{0} \text{ and rank } d\underline{f} < n\} \quad (13)$$

where $d\underline{f}$ is the $n \times (n+1)$ Jacobian matrix of $\underline{f}$ with respect to the state variables, $\underline{u}$, and the bifurcation parameter, λ, but not the parameters $\underline{\alpha}$. The definition of the hysteresis variety is more complicated, but fortunately it is not of great importance for the $r_{max} - Fr_{min}$ problem, since hysteresis occurs only at feed ratios close to the minimum value where we would not design the column.

One result from linear algebra is needed before applying Eq. 13 to the fixed point Eq. 11. For any $m \times n$ matrix A with $m \geq n$, A and $A^T A$ have the same rank ($\leq n$), where $A^T A$ is a

square symmetric $n \times n$ matrix with nonnegative eigenvalues (see, for example, p. 77 of Strang, 1986). A trivial extension says that an $n \times m$ matrix $A^T (m \geq n)$ has the same rank as $A^T A$. Thus, the determinant of $A^T A$ can be used to determine whether A (or A^T) has full rank:

$$\text{rank } A = \text{rank } A^T < n \Leftrightarrow \det(A^T A) = 0 \tag{14}$$

Let $\underline{f}(\underline{x}, r, Fr, q_U, \underline{w}) = \underline{0}$ denote the fixed-point equation for the middle-section map (Eq. 11), where $\underline{f}$ is a vector of dimension $(C-1)$. Then, from Eq. 13 the bifurcation variety is located where $\underline{f} = \underline{0}$ and the rank of the $(C-1) \times C$ matrix $d\underline{f}$ is less than $C-1$. This first criterion is simply the definition of a fixed point. For a ternary mixture $(C=3)$, the second criterion is:

$$\text{rank } (d\underline{f}) = \text{rank} \begin{bmatrix} J_{11} & J_{12} & \dfrac{\partial f_1}{\partial r} \\ J_{21} & J_{22} & \dfrac{\partial f_2}{\partial r} \end{bmatrix} < 2 \tag{15}$$

where J_{ij} are the elements of the $(C-1) \times (C-1)$ Jacobian matrix of $\underline{f}$ with respect to $\underline{x}$, which can be written as:

$$\mathbf{J}_{\underline{f}} = \left[\frac{r + 1 + (q_U - 1) h(Fr, \underline{w})}{r + q_U h(Fr, \underline{w})} \right] Y - I \tag{16}$$

with $Y_{ij} = [\partial y_i / \partial x_j]_{P, \underline{x}'}$.

The partial derivatives $\partial f_i / \partial r$ which appear in $d\underline{f}$ are given by:

$$\frac{\partial \underline{f}}{\partial r} = \frac{h(Fr, \underline{w})(\underline{\hat{y}} - \underline{x}_{F_U}) + (\underline{x}_D - \underline{\hat{y}})}{[r + q_U h(Fr, \underline{w})]^2} \tag{17}$$

Using Eq. 14, the inequality (Eq. 15) is satisfied by requiring:

$$\det [(d\underline{f})^T (d\underline{f})] = (J_{11} J_{22} - J_{12} J_{21})^2 + \left(J_{11} \frac{\partial f_2}{\partial r} - J_{21} \frac{\partial f_1}{\partial r} \right)^2 + \left(J_{12} \frac{\partial f_2}{\partial r} - J_{22} \frac{\partial f_1}{\partial r} \right)^2 = 0 \tag{18}$$

This is equivalent to making the three possible 2×2 determinants of $d\underline{f}$ simultaneously equal to zero. Because of the implicit nature of VLE calculations, Eqs. 11 and 18 must be solved numerically.

One method for calculating $Fr_{\min}$ is to simultaneously solve Eqs. 11 and 18 for the one point that corresponds to the bifurcation variety. In practice, one would first use continuation to locate the limit point on the *SN* branch ($r_{\max}$ for $Fr > Fr_{\min}$) at a particular value of Fr, followed by a simple function evaluation of the determinant in Eq. 18. This process would be repeated at other values of Fr until Eq. 18 is satisfied. (Note that the limit point on the *SN* branch always occurs at a fixed point where Eq. 11 is satisfied.) Because the residual of Eq. 18 is always nonnegative and is zero only at the root, this search is best carried out using minimization techniques rather than root finders, which frequently require the function to change sign at the root in order to work properly.

Note that this method for calculating $Fr_{\min}$ also informally traces out part of the $r_{\max}$ branch as a function of the feed ratio. A better method for calculating $Fr_{\min}$, which formally determines the value of $r_{\max}$ as a function of Fr, is presented in the next section.

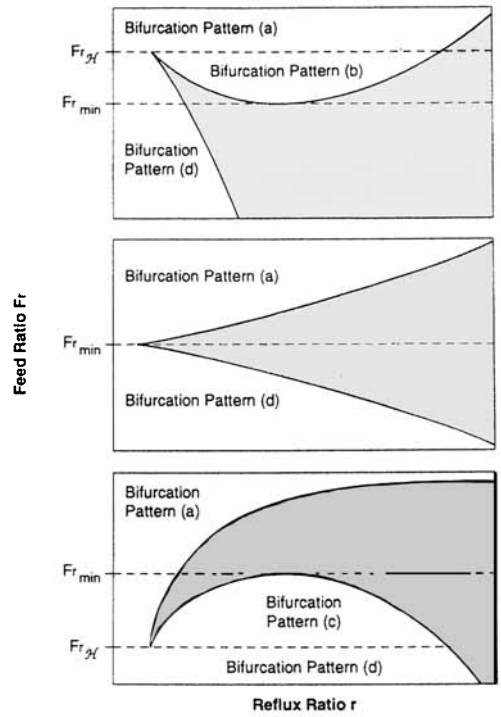

Figure 17. Three possible cusp shapes and their relation to the pitchfork singularity.

The bifurcation patterns correspond to those shown in Figure 16.

Calculating $r_{\max}$ and $Fr_{\min}$: Cusps and Their Interpretation

Because the middle section of any double-feed column, including extractive columns, depends on two parameters, r and Fr, the middle-section fixed points actually define surfaces in the $(C+1)$-dimensional $(\underline{x}, r, Fr)$ space. A useful way of representing these surfaces is to pick out the points on them where the Implicit Function Theorem fails, that is, those points where

$$\underline{f}(\underline{x}, r, F_r) = \underline{0} \tag{19}$$

and

$$\det (\mathbf{J}_{\underline{f}}) = 0 \tag{20}$$

and then project them onto the (r, F_r) plane. The resulting projection yields a cusp-shaped curve such as those shown in Figure 17. One big advantage of this projection is that it eliminates the state variables, and the resulting curves often look the same no matter how many states there are in the model. Since Eqs. 19 and 20 are necessary conditions for a bifurcation to occur, every point on the cusp represents a limit, hysteresis, or bifurcation point. The cusp is thus equivalent to stacking

a family of ($\underline{x}$, r) fixed-point branch figures, each at a different feed ratio, and then projecting their limit, hysteresis, and bifurcation points onto the (r, Fr) plane.

The pitchfork bifurcation and its persistent perturbations in Figure 16, and hence r_{max}, Fr_{min}, and the occurrence of the hysteresis loop in one of the branches can be related to the cusps in Figure 17. These cusps describe the behavior of the $S1$, $S2$, and SN fixed-point branches only (we have not shown the behavior of the UN and SN^- branches). Inside the cusp (the shaded regions in Figure 17), there are three fixed points—$S1$, $S2$, and SN. Outside the cusp (the unshaded regions), there is only one fixed point—either $S1$ or $S2$. Therefore, for $Fr > Fr_{min}$, points which lie in the shaded region correspond to reflux ratios above r_{max}. Different shaped cusps correspond to different sequences of bifurcation diagrams. The cusps can be analyzed either by taking slices at constant feed ratio or at constant reflux ratio. The former is more natural for the $r_{max} - Fr_{min}$ problem.

First, consider the upward-tilting cusp shown at the top of Figure 17. For slices at constant feed ratios, above $Fr_{\mathfrak{BC}}$ there is only one limit point, that is, one intersection with the cusp curve. This is the limit point between $S1$ and SN that determines r_{max}. Therefore, for $Fr > Fr_{\mathfrak{BC}}$, the bifurcation diagram looks like the one in Figure 16(a). Note that the cusp (Figure 17) shows how r_{max} changes with Fr. At $Fr_{\mathfrak{BC}}$, where the tip of the cusp lies, a hysteresis point appears in the $S2$ branch. This corresponds to the bifurcation diagram in Figure 16(a-b) and is equivalent to lying on the hysteresis variety in the bottom of Figure 16. For feed ratios between $Fr_{\mathfrak{BC}}$ and Fr_{min}, there are three limit points. The corresponding bifurcation diagram is Figure 16(b). Reading left to right across Figure 17, the first intersection represents the limit point on the $S2$ branch at the smaller reflux (r_1 in Figure 13a), the second intersection is the other limit point on the $S2$ branch (r_2 in Figure 13a), and the final intersection is the limit point between $S1$ and SN which determines r_{max}. Note how the intersections representing the two limit points on the $S2$ branch move away from each other and how the $S2$-branch limit point at r_2 approaches the $S1$-SN limit point as the feed ratio decreases. At the minimum feed ratio, the intersections representing the $S2$-branch limit point at r_2 and the $S1$-SN limit point coalesce and the cusp curve has zero slope. This corresponds to the bifurcation diagram labeled (b-d) in Figure 16, which is equivalent to lying on the bifurcation variety in the bottom part of Figure 16. Below Fr_{min}, there is again only one limit point and it connects the $S2$ and SN branches. Figure 16(d) is the corresponding bifurcation diagram. In summary, an upward-tilting cusp yields the bifurcation diagrams labeled (a), (a-b), (b), (b-d), and (d) in Figure 16. The diagrams (a-b) and (b-d) are unstable to small perturbations.

A second cusp shape is shown in the middle of Figure 17. Here, the hysteresis and bifurcation points occur simultaneously at the point representing Fr_{min}. This occurs only at the single point (o) in Figure 16 where the two transition varieties cross and corresponds to an unperturbed pitchfork. A perfectly horizontal cusp is represented by the bifurcation diagrams (a), (o), and (d) in Figure 16. Since the unperturbed pitchfork can occur only at the single point where $\mathfrak{B}$ and $\mathfrak{BC}$ meet, it is unstable to small perturbations and represents a transitional case between the upward- and downward-tilting cusps in Figure 17.

The third possible shape is the downward-tilted cusp shown at the bottom of Figure 17. This corresponds to the remaining bifurcation diagrams in Figure 16. For $Fr > Fr_{min}$, the only limit point is between $S1$ and SN, as shown in Figure 16(a). At Fr_{min}, a bifurcation point appears, denoted by a zero slope in the cusp curve, equivalent to lying on $\mathfrak{B}$, and corresponding to the bifurcation diagram (a-c) in Figure 16. Between Fr_{min} and $Fr_{\mathfrak{BC}}$, there are three limit points. The first two are on the $S1$ branch, and the remaining one is where the $S2$ and SN branches coalesce. This region is represented by bifurcation diagram (c) in Figure 16. At $Fr_{\mathfrak{BC}}$ the two limit points on the $S1$ branch coalesce at a hysteresis point. This is equivalent to lying on the hysteresis variety and is represented by bifurcation diagram (c-d) in Figure 16. Below $Fr_{\mathfrak{BC}}$, bifurcation pattern (d) in Figure 16 exists. In summary, a downward-tilted cusp yields bifurcation diagrams (a), (a-c), (c), (c-d), and (d) in Figure 16, Fr_{min} still corresponds to a bifurcation point (crossing $\mathfrak{B}$), and hysteresis still appears, but now it is in the $S1$ branch and only below Fr_{min}.

Of the seven mixtures examined in this study, six yield an upward-tilted cusp, though some of these examples come very close to the untilted cusp. This explains why most of the examples exhibit a hysteresis loop only in the $S2$ branch. Only one of our examples, methanol-acetone-chlorobenzene, results in a downward-tilted cusp.

Because the cusp diagram represents r_{max} at each value of Fr, easily locates Fr_{min} and the hysteresis region, and identifies the fixed-point branch containing the hysteresis loop, a good solution method is to trace out the cusp. This is exactly what two-parameter continuation does. All the cusps shown here were calculated using the built-in two-parameter continuation algorithm in AUTO (Doedel, 1986). In practice, once the feed compositions and a reliable VLE model are given, the desired product purities and feed qualities are set, and an initial value of the feed ratio is chosen, then one-parameter continuation is used to follow the SN branch to its limit point. This limit point then serves as the initial condition for the two-parameter continuation, which traces out the cusp until the final user-specified feed ratio is reached. Fr_{min} and $Fr_{\mathfrak{BC}}$ are automatically identified.

Case Studies

In this section, we demonstrate the above theory for extractive distillations of the mixtures shown in Figures 6, 7, 8 and 9. For each of these mixtures, the components are listed with the product component first, followed by the nonproduct component, and then the entrainer. Only the (x_1, r) projection of the fixed-point branches is shown because this projection is the most useful for recognizing a pitchfork bifurcation and its perturbations. Only the behavior of the $S1$, $S2$, and SN branches is shown in the cusps and most bifurcation diagrams in this section. By convention, stable node branches are denoted by solid lines, while saddle and unstable node branches are denoted by dashed lines.

Example 1

The first example is the acetone-methanol-water separation. The column specifications are given in Knapp and Doherty (1990). The column profile at $Fr = 0.55$ is shown in Figure 6. Figure 18a shows the bifurcation diagram for this mixture at the same feed ratio. For $Fr = 0.55$, $r_{max} = 32.4$, which is far

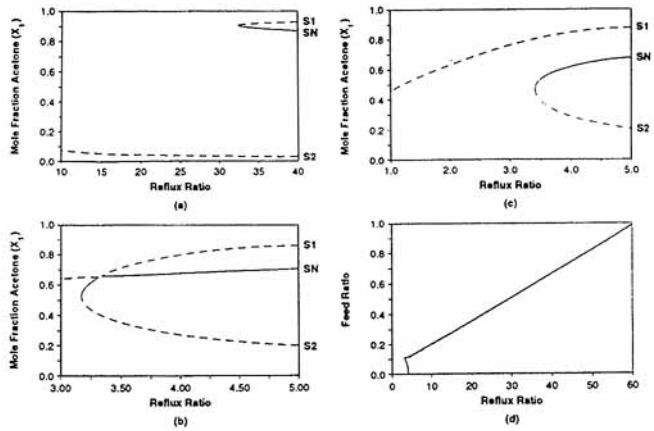

Figure 18. Bifurcation diagrams for the acetone-methanol-water separation: (a) $Fr = 0.55$; (b) $Fr = 0.11334$; (c) $Fr = 0.10$; (d) cusp.

$Fr_{min} = 0.113292$, $r = 3.3212$; $Fr_{3C} = 0.114312$, $r = 3.1333$.

above the operating reflux ratio ($r = 2.76$) used in Knapp and Doherty (1990). Figure 18a is analogous to Figures 12a and 16(a). From Figure 18b it is clear that this mixture does exhibit a perturbed pitchfork bifurcation. This plot at $Fr = 0.11334$ is just slightly above Fr_{min}. The maximum reflux ratio is 3.34 at this feed ratio. Note that the $S2$ branch has a hysteresis loop with limit points at $r = 3.17$ and 3.31, as expected. Figure 18b corresponds to a bifurcation diagram between those shown in Figures 13a and 14a or, equivalently, Figures 16(b) and 16(b–d). The next plot, Figure 18c, at $Fr = 0.10$ is below the minimum entrainer flow—SN meets $S2$, not $S1$, at a limit point. This is analogous to Figure 15a or Figure 16(d). Figure 18d shows the upward-tilting cusp in (r, Fr) space for this example. This figure summarizes the information contained in the previous three

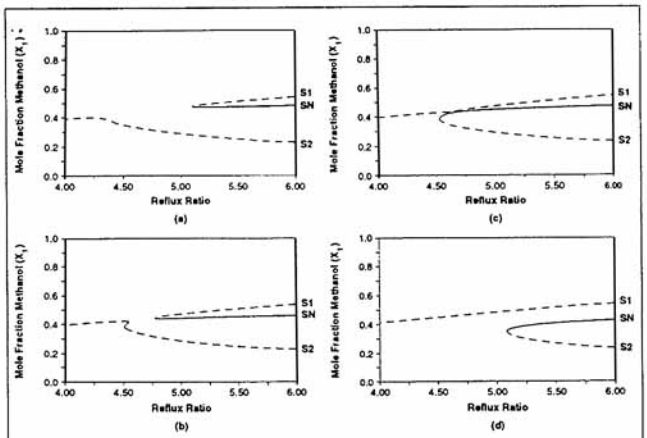

Figure 19. Bifurcation diagrams for the methanol-acetone-MEK separation: (a) $Fr = 0.735$; (b) $Fr = 0.730$; (c) $Fr = 0.7291$; (d) $Fr = 0.70$; (e) cusp.

$Fr_{min} = 0.729172$, $r = 4.6613$; $Fr_{3C} = 0.730904$, $r = 4.485$.

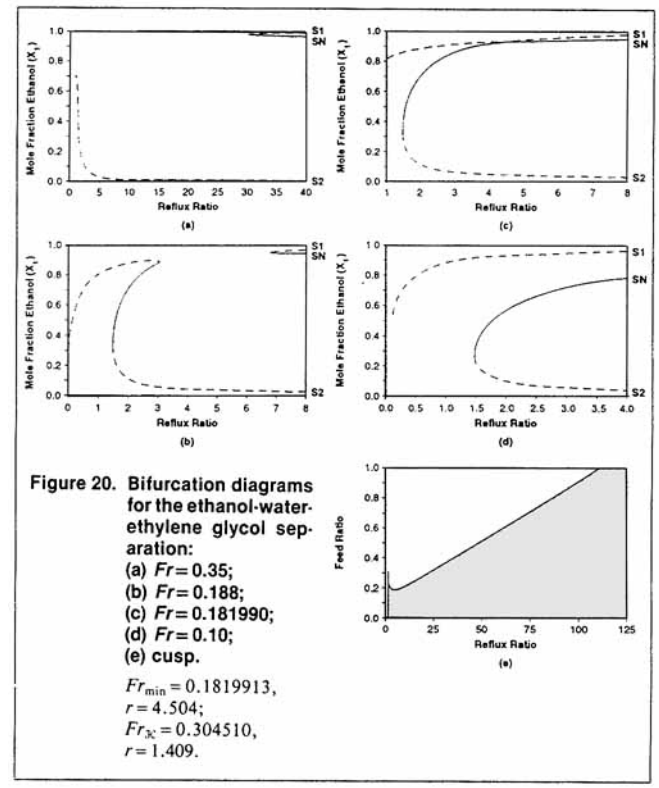

Figure 20. Bifurcation diagrams for the ethanol-water-ethylene glycol separation: (a) $Fr = 0.35$; (b) $Fr = 0.188$; (c) $Fr = 0.181990$; (d) $Fr = 0.10$; (e) cusp.

$Fr_{min} = 0.1819913$, $r = 4.504$; $Fr_{3C} = 0.304510$, $r = 1.409$.

plots, and enables the maximum reflux ratio at any feed ratio to be simply read off of the plot. Although it is hard to see, the cusp is tipped slightly upward. The $S2$ branch starts to show hysteresis at $Fr = 0.1143$. The minimum feed ratio is 0.1133.

Example 2

The second example is the methanol-acetone-MEK separation at 10 atm from Knapp and Doherty (1992). Note that at this pressure the azeotrope between methanol and MEK has disappeared, and the only azeotrope in the system is the one between methanol and acetone, which we are breaking by extractive distillation. The column specifications at $Fr = 1.7$ are given in Figure 4.13 and Table 4.5 of Knapp (1991) with the corresponding column profile in Figure 9. Figures 19a–19d confirm that this mixture also exhibits a perturbed pitchfork bifurcation and follows the progression of bifurcation diagrams in Figures 12 to 15, and 16(a), 16(b), and 16(d).

Figures 19a–19d demonstrate that the transition from the behavior in Figure 12 to the behavior in Figure 15 can take place over a narrow range of feed ratios. At $Fr = 0.735$ (Figure 19a), there is no hint of a hysteresis loop, yet by $Fr = 0.730$ (Figure 19b) the $S2$ branch has two limit points. A further small change in feed ratio to $Fr = 0.7291$ (Figure 19c) results in a bifurcation diagram below Fr_{min}. (This figure is drawn very close to the pitchfork at Fr_{min}. Although it may be difficult to see, the $S1$ branch does not touch the SN branch so this feed ratio is indeed below Fr_{min}.) By $Fr = 0.70$ (Figure 19d), there is no longer any evidence that the pitchfork bifurcation existed. Because all of these changes occur over such a narrow range of feed ratios, one might correctly guess that the corresponding cusp shows very little deviation from the horizontal

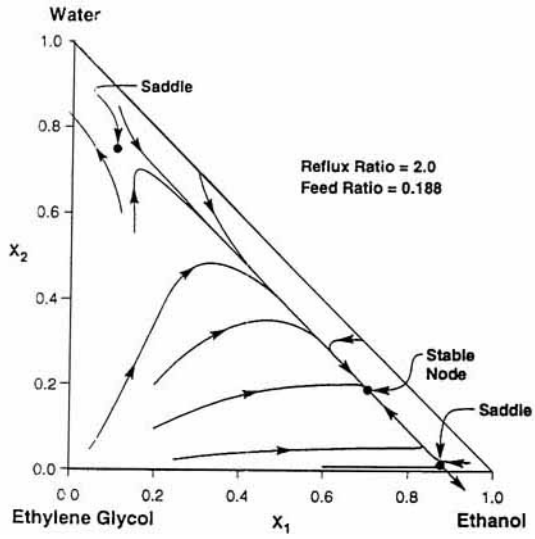

Figure 21. Phase plane for the middle-section map showing the three fixed points on the *S2* branch in the hysteresis region.

(see Figure 19e). Although it is not apparent from the figure, this cusp does in fact tilt slightly upward. Hysteresis exists in the *S2* branch only over the narrow range from $Fr_{3C} = 0.7309$ to $Fr_{min} = 0.7292$.

Example 3

The third example is the ethanol-water-ethylene glycol separation discussed in Knapp and Doherty (1990). Like the previous two examples, this mixture also exhibits the perturbations of the pitchfork bifurcation consistent with an upward-tilted cusp (see Figures 20a–20d). Despite its appearance, Figure 20c at $Fr = 0.181990$ is not quite at Fr_{min}, although it is about as close as one can get.

Unlike the other examples, however, hysteresis in the *S2* branch exists over a wide range of feed ratios from $Fr_{3C} = 0.30451$ to $Fr_{min} = 0.181991$, as can be seen from the highly tilted cusp in Figure 20e. As mentioned earlier, this complicates the behavior of the middle-section map. Referring to Figure 20b at $Fr = 0.188$, the separation is infeasible above $r_{max} = 6.79$ because (1) the middle-section trajectories are attracted to *SN*, which lies inside the triangle, and (2) the separatrices associated with *S1* prevent any middle-section trajectories from reaching the rectifying profile. Between $r_{max} = 6.79$ and $r = 3.07$, where a limit point occurs on the *S2* branch, it is possible to design a feasible column because there is no longer a stable node inside the composition space nor a separatrix blocking access to the rectifying profile. At all reflux ratios between $r = 1.48$ and $r = 3.07$, there are three fixed points on the *S2* branch—two saddles and one stable node. Figure 21 shows the location of these fixed points at $r = 2.0$. Because another stable node exists inside the triangle for this range of reflux ratios and because of the separatrices connected to the new saddle (the one lying near the ethanol vertex in Figure 21), the separation once again becomes infeasible. This is entirely analogous to being above r_{max}. Compare the location of the fixed points in Figure 21 with those in the phase plane above r_{max} in Figure 10a. The only fundamental difference between these two figures is that the three fixed points in Figure 21 all lie on the same fixed-point branch. Of course, this is not apparent without Figure 20b. Theoretically, the separation again becomes possible below the hysteresis region ($r_{min} < r < 1.48$), but, because of the location of the saddle which remains, it is unlikely that the separation in this example would be feasible in this range. From a design engineer's perspective it is important to know where hysteresis exists and how it complicates the feasibility of a desired separation to ensure that one does not design a column which operates near this region.

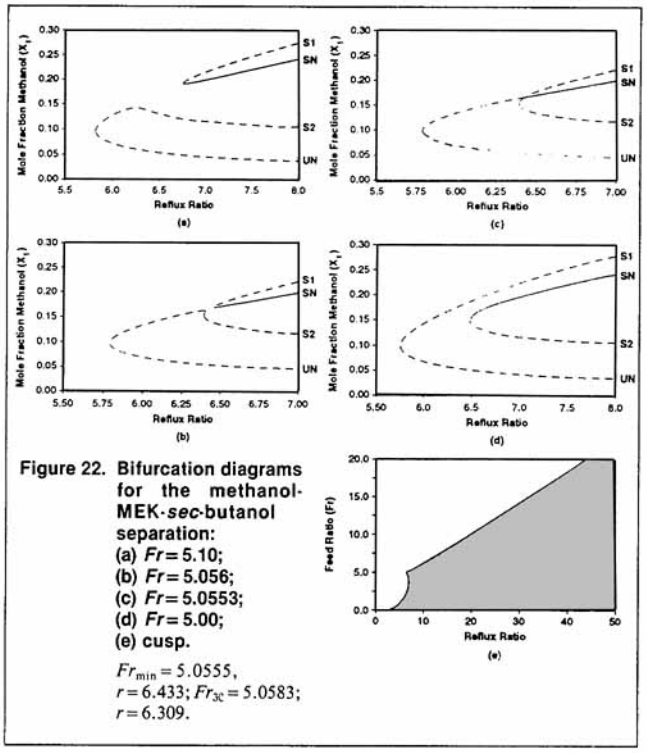

Figure 22. Bifurcation diagrams for the methanol-MEK-*sec*-butanol separation:
(a) $Fr = 5.10$;
(b) $Fr = 5.056$;
(c) $Fr = 5.0553$;
(d) $Fr = 5.00$;
(e) cusp.

$Fr_{min} = 5.0555$, $r = 6.433$; $Fr_{3C} = 5.0583$; $r = 6.309$.

Example 4

The final example is the separation of methanol and MEK using *sec*-butanol as the entrainer. The column profile and column specifications at $Fr = 15$ are shown in Figure 8. Figures 22a–22d show that this mixture also follows the progression of bifurcation diagrams in Figures 12 to 15 and therefore also results in an upward-tilting cusp (Figure 22e). Like the first two examples, the hysteresis region is so narrow (between $Fr_{3C} = 5.0583$ and $Fr_{min} = 5.0555$) that the cusp appears virtually horizontal. Note how much higher the value of Fr_{min} for this mixture is compared to the previous examples.

The feature that sets this example apart from the previous three is the inclusion of the *UN* branch and its limit point on the bifurcation diagrams in Figures 22a–22d. The cusp in Figure 22e still represents the behavior of the *S1*, *S2*, and *SN* branches only. As shown in part b of Figures 12 to 15, *UN* always forms a limit point with either *S2* or *S1*, but this limit point usually occurs at reflux ratios far below those at which the more important interactions between the *S1*, *S2* and *SN* branches take place. That is why the *UN* branch and its limit point are not shown in the other examples, though the connection with the *UN* branch is hinted at in Figures 20b and

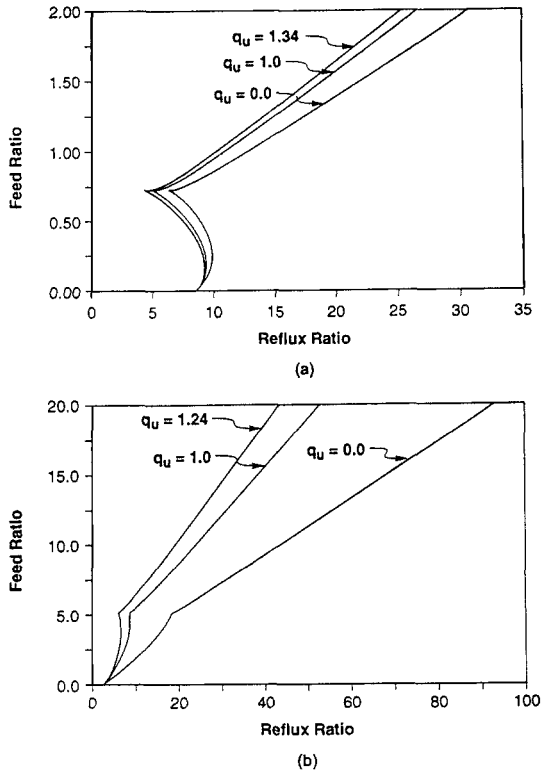

Figure 23. Effect of q_U on Fr_{min} and r_{max}: (a) methanol-acetone-MEK separation; (b) methanol-MEK-*sec*-butanol separation.

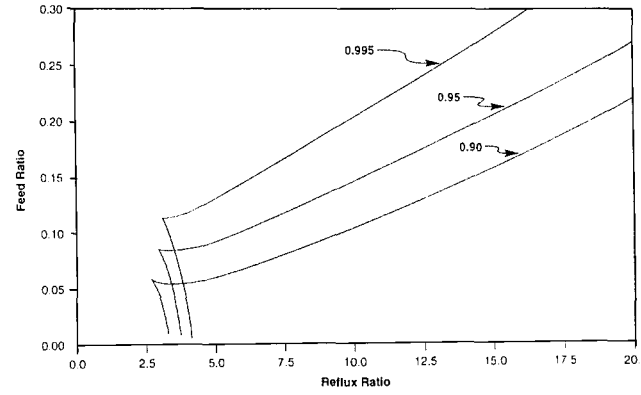

Figure 24. Effect of the distillate purity on Fr_{min} and r_{max} for the acetone-methanol-water example.

20d. Thus, Figures 22a-22d actually give a more complete picture of the solution space of the middle-section map than the previous examples. These figures also show how the *UN* branch switches from meeting *S*2 at a limit point to meeting *S*1 at a limit point as Fr_{min} is crossed (as *SN* switches from meeting *S*1 to meeting *S*2 at a limit point).

Parametric Sensitivity

So far, the analysis has been confined to a single (isolated) extractive distillation column where we have kept many of the parameters at fixed values. These columns, however, are normally part of a sequence in which the entrainer is recycled back to the extractive column. It is of interest, therefore, to explore the sensitivity of our results to changes in parameters, especially parameters such as the feed quality of the entrainer feed (q_u) which may vary due to downstream process fluctuations. The fixed-point equation for the middle section, Eq. 11, depends on the parameters r, Fr, q_U, $\underline{x}_D$, $\underline{x}_B$, $\underline{x}_{F_U}$, $\underline{x}_{F_L}$, the column pressure, and the VLE model used. To this point, r and Fr have been allowed to vary with all of the other parameters held fixed. The purpose of this section is to briefly explore the effect that other selected parameters have on r_{max} and Fr_{min}. We assume that the process feed composition, $\underline{x}_{F_L}$, is fixed due to upstream process constraints and that the VLE model was chosen because it accurately represents the available experimental data. The upper feed ($\underline{x}_{F_U}$) is necessarily nearly pure entrainer (see pp. 164-165 of Knight, 1986) and thus cannot change significantly. Unless the extractive column is part of a pressure-swing distillation sequence or a sequence that is to be thermally-integrated, the effect of varying pressure is not likely to be of great interest. Of the remaining parameters, only the effect of varying feed quality, q_U, and product purity, $x_{D,1}$, have been examined.

In practice, the upper feed of extractive distillations is typically subcooled ($q_U > 1.0$). For the purpose of the parametric study, the upper-feed quality was allowed to vary between 0.0 and 2.0. For every example studied, the upper-feed quality had no effect on the minimum feed ratio or on the feed ratio marking the onset of hysteresis. The value of q_U, however, does affect the relationship between r_{max} and Fr. The trend is always the same. For a given feed ratio, r_{max} occurs at higher reflux values as q_U decreases and this effect is magnified at larger feed ratios (see Figure 23). There is a simple explanation for this.

Maximum reflux occurs when the internal reflux in the middle section reaches a certain value. The middle-section reflux comes from two sources: (1) the reflux from the rectifying section (the external reflux for CMO columns) and (2) the upper feed. A subcooled upper feed provides some additional reflux in the middle section, thereby reducing the external reflux ratio corresponding to r_{max} (that is, the external reflux ratio necessary to achieve the required middle-section reflux). As the feed quality decreases (that is, the upper feed is less subcooled or even partially vaporized), the upper feed's contribution to the internal flow is smaller and the external reflux ratio must increase to maintain the same internal reflux ratio in the middle section. Hence, r_{max} occurs at larger external reflux ratios as q_U decreases. This effect is quantified by Eq. A10, which becomes:

$$r_M = r + q_U \frac{F_U}{D} \tag{21}$$

after dividing by D. Equation 21 also shows why r_{max} is shifted more as Fr (and thus F_U) increases. Figure 23 shows the effect of the upper-feed quality on maximum reflux and how this effect depends on the feed ratio (see especially Figure 23b). Note that, as expected, q_U has no effect as Fr goes to zero. The feed, distillate, and bottoms compositions also influence the effect of q_U on r_{max}, as quantified by Eq. 21 via Eq. A9.

The distillate purity, as expressed by $x_{D,1}$, affects not only r_{max}, but also Fr_{min} (see Figure 24). As the distillate purity increases, Fr_{min} and Fr_{3C} increase, but, for a fixed feed ratio,

r_{max} decreases. The influence of $x_{D,1}$ on Fr_{min} conforms with intuition. As the distillate purity increases, the separation becomes more difficult and more entrainer is required. For example, in the acetone-methanol-water separation, the minimum feed ratio increases from 0.0545 to 0.1133 as $x_{D,1}$ changes from 0.90 to 0.995.

Predicting Which Pure Component Is the Distillate

Since acetone boils at a lower temperature than methanol (56.1°C vs. 64.5°C at 1 atm), it is logical to expect that acetone will be recovered as the distillate product in an extractive distillation. When water is used as the entrainer, this is indeed what happens (see Figure 6 and Knapp and Doherty, 1990). When the entrainer is MEK, however, either the higher boiling MEK-methanol azeotrope (64.2°C at 1 atm) or pure methanol, not acetone, is the distillate product depending on the pressure (see Figure 9 and the discussion on p. 354 of Knapp and Doherty, 1992).

The seemingly unusual phenomena of having an intermediate-boiling azeotrope or pure component, rather than the lowest-boiling component, distill overhead in the extractive column has actually been known for over 40 years and has been observed for a number of mixtures and entrainers. For example, the extractive distillation of ethanol and water with gasoline (Black, 1980), some phenols (Zudkevitch et al., 1984a), cyclic ketones, cyclic alcohols (Zudkevitch et al., 1984b), or one of the various compounds cited by Berg and Yeh (1986, 1987) causes water to be removed as the overhead product of the extractive column and the lower-boiling ethanol to leave in the bottom stream with the entrainer. Scheibel (1948), Berg and Yeh (1985a), and Yeh et al. (1988) state that the higher ketones will distill methanol overhead from methanol-acetone mixtures. (Unlike the others, Scheibel (1948) correctly states that MEK is not suitable for extractive distillation at 1 atm because of the existence of a minimum boiling azeotrope between MEK and methanol.) Buell and Boatright (1947) found that furfural would reverse the natural volatility of butene-butadiene mixtures. Kolbe et al. (1979) showed that aniline or nitrobenzene would cause the intermediate-boiling cyclohexane to be recovered overhead from benzene-cyclohexane mixtures. Berg and Yeh (1985b) found that DMSO caused the higher-boiling ether to become the distillate when distilling acetone and isopropyl ether. Scheibel (1948) also lists potential extractive entrainers to make the higher-boiling component distill overhead from acetone-chloroform and ethanol-ethyl acetate mixtures. Since it is possible for either the light or the intermediate component to be the distillate product depending on the entrainer chosen, the obvious question is: "How does one correctly predict which component will be the product?" There are several ways of answering this question. Since the product component is determined strictly by thermodynamics, this question can always be answered before starting any column design calculations.

According to Scheibel (1948), the answer lies in the effect of the entrainer on the relative volatility of the components of the azeotrope. In nonideal mixtures at low to moderate pressures, the relative volatility is expressed by:

$$\alpha_{12} = \frac{\gamma_1 P_1^{sat}}{\gamma_2 P_2^{sat}} \tag{22}$$

where component 1 represents the lower-boiling pure component. Entrainers are selected to behave essentially ideally with one of the components and to cause positive or negative deviations from Raoult's law with the other component. If the selected entrainer is essentially ideal with component 1 and causes positive deviations from Raoult's law for component 2 ($\gamma_1 \sim 1$ and $\gamma_2 > 1$), or the selected entrainer is essentially ideal with respect to component 2 and causes negative deviations from Raoult's law for component 1 ($\gamma_2 \sim 1$ and $\gamma_1 < 1$), then, depending on the ratio of the vapor pressures, the higher-boiling pure component 2 can be more volatile than the lower-boiling pure component 1 ($\alpha_{12} < 1$) and component 2 may become the distillate. Scheibel (1948) attributes these positive and negative deviations from ideality to hydrogen bonding and suggests using a homolog of one of the azeotropic components to hopefully force the other component overhead. Ewell et al. (1944) divide liquids into five classes based on their potential for forming hydrogen bonds and show how interactions between these groups affect deviations from Raoult's law. Berg (1969) states that successful extractive entrainers are highly hydrogen-bonded liquids of class I or II.

Robinson and Gilliland (1950) use polarity arguments to explain the increase or decrease in relative volatility caused by the addition of an entrainer. "The general rule is (1) if the added material is more polar than the components of the original mixture, it will increase the relative volatility of the less polar component relative to the more polar, and (2) if the added material is less polar, the reverse will be true" (p. 288). As an example, they cite using polar water to separate the less polar acetone from the more polar methanol. "While theoretically it is possible to add a material of either higher or lower polarity, both cases are not usually equally attractive or practical" (p. 289). Because of the natural difference in vapor pressures between the azeotropic constituents, an entrainer which enhances this "natural volatility difference" (increases γ_1 relative to γ_2 when $P_1^{sat} > P_2^{sat}$) is favored over one which increases γ_2 relative to γ_1. In this latter case, "adding small quantities of the agent [entrainer] actually makes the separation more difficult, and large enough quantities must be used to reverse the normal volatility completely" (p. 289). Translated into the terminology used here, the former case will have a lower value of Fr_{min} than the latter. The above methods allow the designer to make an educated guess for which component will be the distillate product, though these methods are by no means infallible.

For ternary mixtures there is another method that has been used for many years to determine the product component, namely, pseudo-binary y-x phase diagrams (for example, p. 297 of Robinson and Gilliland, 1950; Kolbe et al., 1979). A pseudo-binary phase diagram is one which plots the VLE data for the azeotropic constituents (components 1 and 2) on an entrainer-free basis. With no entrainer present, the pseudo-binary y-x diagram is the true binary y-x diagram (Figure 25a). At the azeotrope, where the VLE curve crosses the 45° line, $\alpha_{12} = 1.0$. To determine which component is the distillate, a series of pseudo-binary y-x plots must be drawn at increasing entrainer concentrations until the pseudo-azeotrope (the point where the entrainer-free VLE curve crosses the 45° line or where $\alpha_{12} = 1.0$) disappears into one of the pure-component corners. (This can be formulated as a bifurcation problem as discussed in Knapp, 1991.) The resulting pseudo-binary phase

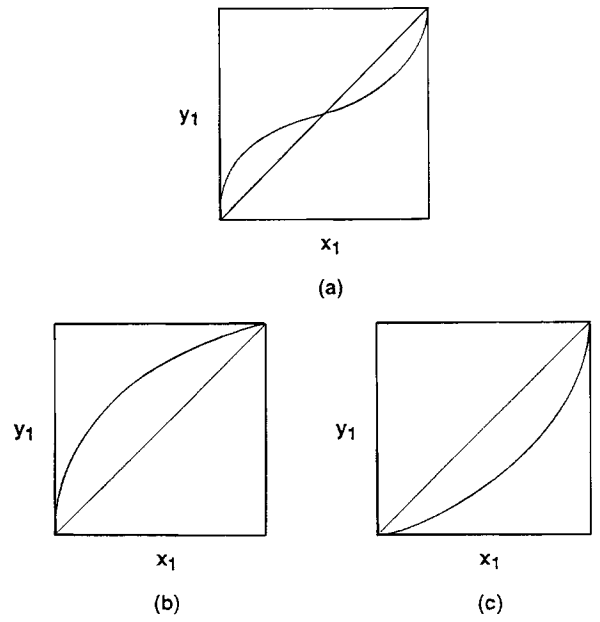

Figure 25. Using pseudo-binary (entrainer-free) *y-x* phase diagrams to determine which component will be the distillate product.

(a) No entrainer; (b) sufficient entrainer to eliminate the pseudo-azeotrope; component 1 will be the distillate; (c) the same as (b) except component 2 will be the distillate.

diagram will be either the one in Figure 25b or Figure 25c. The expressions to "break" or "negate" an azeotrope originated from the use of these pseudo-binary phase diagrams because that is what appears to happen as the entrainer concentration increases. Figure 25b indicates that the entrainer increases the volatility of component 1 relative to component 2 so that component 1 will be the distillate product. If the resulting pseudo-binary *y-x* diagram is the same as Figure 25c, then the entrainer has the opposite effect and component 2 will be the distillate. The pseudo-binary *y-x* phase diagrams can also be used to make a rough qualitative comparison between entrainers. The smaller the mole fraction of entrainer required to make the pseudo-azeotrope disappear, the better the entrainer (and the lower the corresponding value of Fr_{min}) should be. Laroche et al. (1991) provide an alternative implementation of this approach where the locus $\alpha_{12} = 1.0$ is tracked on the composition triangle. To make a quantitative comparison, Fr_{min} needs to be calculated for each candidate entrainer.

It is also possible to predict the product component using the fixed-point techniques developed in this article. When acetone is guessed to be the distillate in the methanol-acetone-MEK mixture, the *SN* branch meets the *S*2 branch from the methanol vertex at a limit point (Figure 26a). This is the same fixed-point branch behavior observed for infeasible separations below Fr_{min}. Consequently, acetone cannot be the distillate product. In contrast, when methanol is selected to be the distillate (Figure 26b), the *SN* branch meets the *S*1 branch from the methanol vertex at a limit point. This is the middle-section fixed-point geometry for feed ratios above the minimum which gives rise to feasible extractive distillations. Thus, methanol is the distillate. (Note that the triangles in Figure 26 are always drawn in the standard orientation, that is, with the suspected product component in the lower righthand corner.) This be-

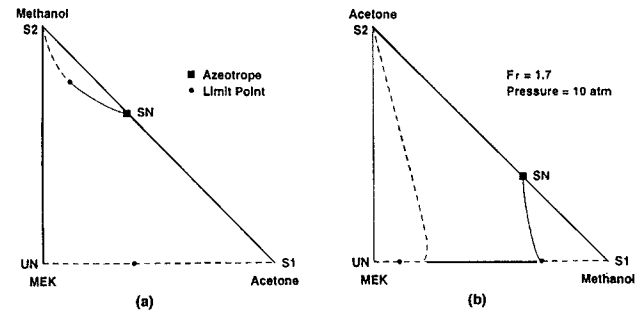

Figure 26. Using fixed-point branches to determine which component will be the distillate product.

(a) Acetone is not the correct product because the *SN* branch meets the *S*2 branch at a limit point; (b) methanol is the distillate product because the *SN* branch meets the *S*1 branch at a limit point.

havior was observed for every mixture examined and explains why only one of the two azeotropic constituents can be recovered in an extractive distillation column with a given entrainer, despite the symmetry of the residue-curve map (see Figure 5). When the wrong component is selected as the distillate, the *SN* and *S*2 branches form a limit point at *all* feed ratios, and when the correct component is selected as the distillate, the *SN* and *S*1 branches form a limit point for $Fr > Fr_{min}$. This fixed-point method should easily extend to mixtures with four or more components.

Implications for Design and Control

We have shown that a maximum reflux ratio and a minimum feed ratio exist for every extractive distillation. In addition, it is well known that some entrainers cause the intermediate-boiling pure component to distill overhead. The fixed-point branches of the middle-section map provide a unifying framework for understanding these phenomena. In fact, *tracking the behavior of the stable node (SN) branch which originates at the azeotrope is sufficient to locate r_{max} and Fr_{min}, and to determine which component must be the distillate product.*

(1) If *SN* forms a limit point with the saddle *S*2 from the "nonproduct" vertex, then the feed ratio is below the minimum or the wrong component was selected as the product. The minimum feed ratio corresponds to a bifurcation point where the *SN*, *S*2, and *S*1 (the saddle from the "product" vertex) branches meet.

(2) If *SN* forms a limit point with *S*1, then the correct component was selected as the product, the feed ratio is above the minimum, and the maximum reflux ratio for this value of the feed ratio is the reflux ratio at which the limit point occurs.

(3) If the *SN* branch no longer meets *S*1 or *S*2 at a limit point, but instead proceeds to the base of the composition triangle, then there has been a transition in the defining condition for maximum reflux (see Appendix B). Maximum reflux now corresponds to the reflux ratio at which the *SN* branch crosses the location of the rectifying profile.

It is common knowledge that the number of trays becomes infinite at the minimum reflux ratio, but in addition *at fixed product purities*, after decreasing to a minimum, the required number of trays starts to increase with increasing reflux ratio until it once again becomes infinite at the maximum reflux

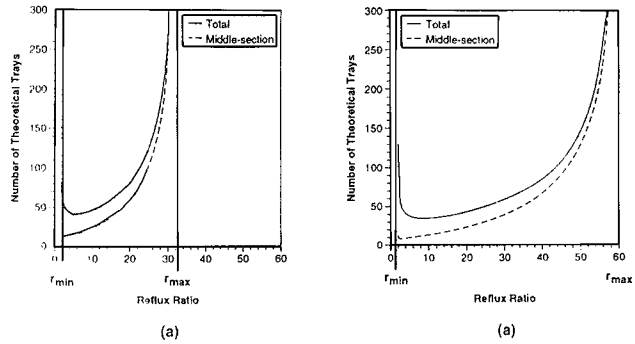

Figure 27. Number of theoretical trays as a function of the reflux ratio for the acetone-methanol-water separation.

(a) Feed ratio = 0.55; (b) feed ratio = 1.0.

ratio (Figure 27). Note that the number of trays starts to increase at relatively small values of r, not far beyond r_{min}. Two different effects cause the infinite number of trays at r_{min} and r_{max}. For sharp, direct splits in a double-feed column (such as extractive distillation of a minimum-boiling azeotrope), the number of trays in the stripping section becomes infinite at minimum reflux (Levy and Doherty, 1986a), because the stripping-section stable node (the feed pinch in that article's terminology) lies on the middle-section profile. If the minimum reflux is caused by a tangent pinch in the rectifying section, then the number of trays in the rectifying section becomes infinite at r_{min}. In contrast, as can be seen in Figure 27, the number of trays in the *middle section* becomes infinite at the maximum reflux ratio. This is due to the appearance of the *SN-S1* limit point at r_{max}.

From a design perspective, an engineer would select a reflux ratio that requires fewer trays. From an operation or control perspective, an engineer wants a flexible column that can continue to produce the desired product over a range of operating parameter values. In most distillations, the number of trays required to achieve a given separation decreases monotonically as the reflux ratio increases. Consequently, a common control action to maintain product purity is to increase the internal flows, for example, by increasing the boilup rate and/or the reflux ratio. The occurrence of a maximum reflux ratio (and indirectly a maximum reboil ratio) and the accompanying increase in trays at increasing reflux have serious implications for the control of extractive distillation columns because at some value of r not far above r_{min} a further *increase* in reflux causes a *decrease* in product purity. Above this point, a *decrease* in reflux is needed to *increase* the product purity. Anderson et al. (1989) also observed an inverse response to increased internal flows at low feed ratios. At the controller design stage, the number of trays has already been fixed. Therefore, if the number of trays necessary to achieve a desired product purity increases as the reflux increases, the column will not be able to produce the desired product at higher reflux ratios. Thus, it is vital to know at what reflux ratio this effect begins so that the column and the control system can be designed correctly.

Assuming that Figure 27 represents the number of trays required to achieve the desired product specifications, a column designed at a feed ratio of 1.0 (Figure 27b) would be more flexible than one designed at $Fr = 0.55$ (Figure 27a), because

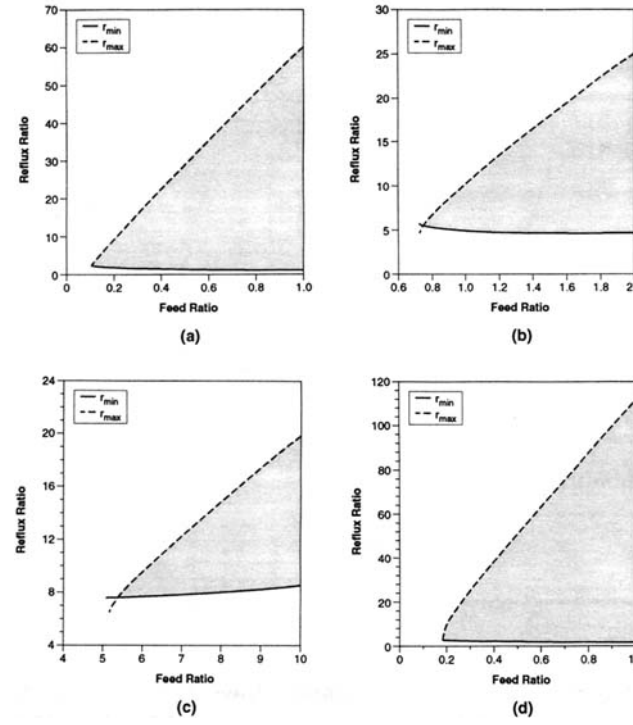

Figure 28. Minimum and maximum reflux ratios as a function of the feed ratio.

The shaded region is the potential operating reflux range. (a) Acetone-methanol-water separation; (b) methanol-acetone-MEK separation; (c) methanol-MEK-*sec*-butanol separation; (d) ethanol-water-ethylene glycol separation.

the former has a wider range of reflux ratios that requires about the same number of trays than the latter. In other words, the desired product specifications can be maintained over a wider range of reflux ratios as the feed ratio increases. Another way to see that the range of operating reflux ratios increases with feed ratio is to plot r_{min} and r_{max} as functions of the feed ratio (Figure 28). The minimum and maximum reflux ratio branches are not required to meet and end at Fr_{min} because each quantity is calculated from completely different constructions using different fixed points (a limit point between the middle-section *S1* and *SN* branches for r_{max} vs. the collinearity [zero volume] of the stripping-section stable node, the middle-section *S2* saddle and the feed point, for r_{min}). Consequently, there is nothing wrong with the two curves crossing. Of course, the only physically-meaningful region is where $r_{max} > r_{min}$. Since the number of trays becomes infinite at both r_{min} and r_{max}, the actual operating range (the range requiring approximately the same number of trays to achieve the desired product purities) is somewhat smaller than the shaded region in the figures. (The common heuristic, $r_{op} = 1.2$ to $1.5\ r_{min}$ is adequate for locating the lower bound of this range.) Moreover, the region in which the number of trays decreases with increasing r, where we can expect good control, is very much smaller than the shaded region.

From the control engineer's point of view, relatively large values of feed ratio yield the simpler control properties associated with ordinary distillations (Andersen et al., 1989). The number of trays in the middle section, and hence the column, becomes infinite as Fr_{min} is approached (Figure 29), but rapidly decreases before reaching an asymptote or slowly

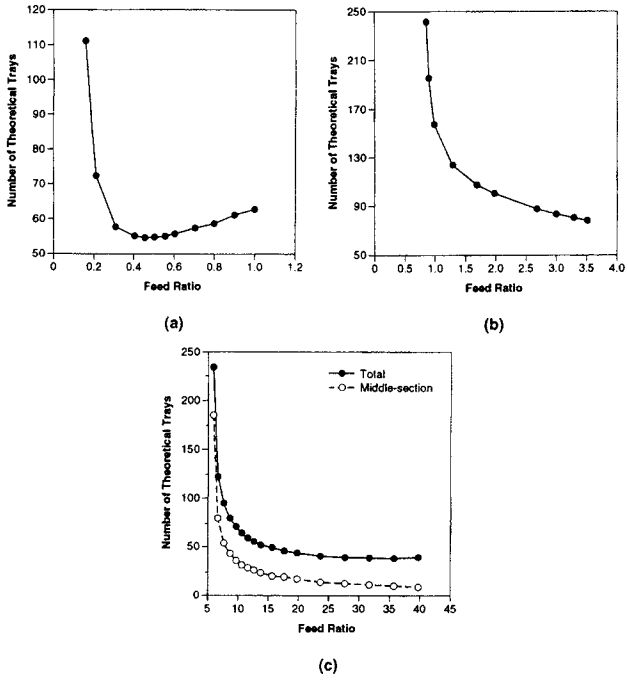

Figure 29. Number of theoretical trays in the extractive distillation column as a function of the feed ratio at reflux ratios of 1.2 r_{min}.

(a) Acetone-methanol-water separation; (b) methanol-acetone-MEK separation; (c) methanol-MEK-*sec*-butanol separation.

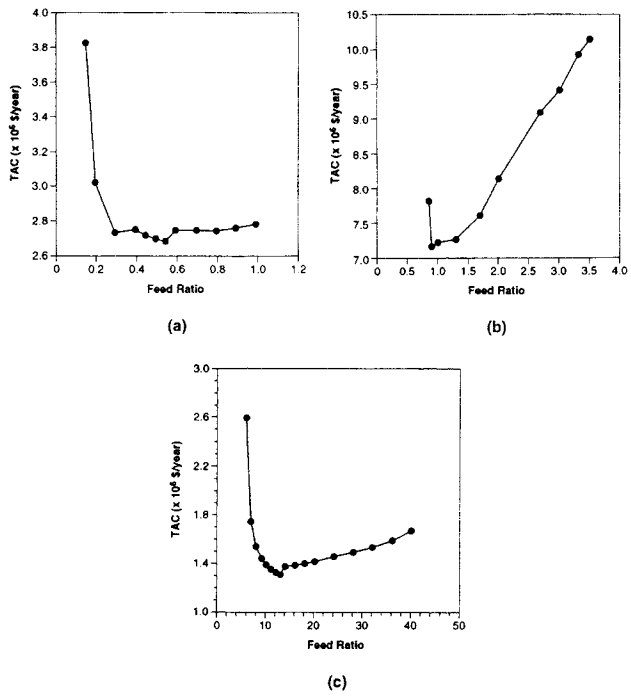

Figure 30. Extractive distillation sequence cost as a function of the feed ratio at reflux ratios of 1.2 r_{min}.

(a) Acetone-methanol-water separation; (b) methanol-acetone-MEK separation; (c) methanol-MEK-*sec*-butanol separation (extractive column only).

increasing, as the feed ratio increases. This too suggests designing extractive columns to operate away from Fr_{min}. On the other hand, a larger feed ratio requires larger column diameters and larger heat duties in both the extractive and entrainer-recovery columns which lead to higher capital and operating costs. This suggests using a small feed ratio. Thus, there must be some compromise between the number of trays, and the column diameters and energy requirements. From Knight and Doherty (1989) and Knapp and Doherty (1990), we know that the feed ratio is always one of the variables with the greatest effect on the total separation cost. Thus, it is always important to find an economical value of the feed ratio. Figure 30 shows how the feed ratio affects the total annualized cost (TAC) of the entire sequence. The TAC is calculated by the method described in Knapp and Doherty (1990). Figure 7 of Knight and Doherty (1989) shows the same information for the ethanol-water-ethylene glycol separation. (While the trend is unchanged, their costs must be approximately doubled to correct an error in their cost model—see Knapp and Doherty, 1990.) For every example, the cost is infinite at Fr_{min}, quickly decreases to near minimal cost over a range of feed ratios, and then slowly increases again at "large" feed ratios. Therefore, from the design perspective, the column should be built to operate in the basin of near minimal cost by selecting a feed ratio near the economically optimum value. Jacobsen et al. (1991) indicated that with the right control system configuration and with properly tuned controllers, extractive distillation columns operating at economically optimum values of the feed ratio are no more difficult to control than ordinary distillation columns with high-purity products.

Since the feed ratio is often the only dominant optimization variable, a heuristic for selecting the most economical feed ratio would be useful for conceptual design purposes or as a starting point for a final design. Unfortunately, there are only five examples for which cost vs. feed ratio data exist in the literature (see Table 1). While this is not sufficient for developing a heuristic, we should nevertheless make the most of it. If we write the optimal feed ratio, which gives the minimum cost as:

$$Fr_{optimum} = \sigma Fr_{min} \tag{23}$$

then, based on the data in Table 1, $\sigma \cong 1.5$ to 2.5. If the goal is to find an operating value of the feed ratio, Fr_{op}, that gives a low-cost design within 10–15% of the minimum, rather than the most economical feed ratio, then the guideline is:

$$Fr_{op} = \delta Fr_{min} \tag{24}$$

where, based on the data in Table 1, $\delta \cong 2.0$ to 4.0. As more

Table 1. Optimal Feed Ratios as a Multiple of the Minimum Feed Ratio

Separation	Fr_{min}	$Fr_{optimum}$	σ	δ
Methanol-MEK-*sec*-butanol	5.056	13.0	2.6	1.8 to 4.5
Methanol-acetone-MEK	0.729	0.90	1.23	1.2 to 2.6
Ethanol-water-ethylene glycol	0.182	0.50	2.7	2.5 to 8.3
Acetone-methanol-water	0.113	0.55	4.9	2.6 to 8.8
Proprietary mixture	0.480	0.80	1.67	1.4 to 2.7

$Fr_{optimum} = \sigma Fr_{min}$; $Fr_{op} = \delta Fr_{min}$

Reported ranges of δ are based on values of Fr that yield designs with a TAC within 10% of the optimum.

examples are studied, the reliability of these guidelines will improve. At the present state of the art, the design engineer should still do several preliminary designs at feed ratios both inside and outside of the recommended ranges. Because of the steep rise in cost near Fr_{min}, it is always safer to err on the high side.

As useful as residue-curve maps are for identifying feasible entrainers, they cannot be used to differentiate between entrainers yielding the same map. Thus, the correct residue-curve map is a necessary condition for a good extractive entrainer, but it is not a sufficient condition. Although they all have the same residue-curve map and they all give feasible designs, not all candidate entrainers give practical or economical designs. Up to now, the only reliable way to discriminate between feasible entrainers was to design and optimize the distillation sequence for each entrainer and to compare their costs, which is a very time-consuming task. Because the feed ratio is always one of the variables with the greatest effect on the sequence cost, an entrainer with a smaller optimal feed ratio is preferred over one with a much larger optimal feed ratio. Unfortunately, rigorously determining $Fr_{optimum}$ requires designing and optimizing extractive distillation sequences, which offers no advantage over the existing method. The next best thing to comparing optimal feed ratios is to compare minimum feed ratios. An entrainer with a smaller minimum feed ratio can be expected to have a smaller optimal feed ratio, as demonstrated by the examples in Table 1. Thus, minimum feed ratios can be used in a second-level screening of candidate entrainers that have passed the residue-curve-map test. A big advantage of this approach is that the minimum feed ratio for each entrainer can be calculated quickly using the method developed above and the list of potential entrainers can be pared down without the need for any column design calculations.

The second-tier screening of the set of feasible extractive entrainers proceeds as follows:

1. Pick a cutoff point for the minimum feed ratio, say $Fr = 1.0$. Any entrainer with a minimum feed ratio greater than this cutoff value will be discarded as uneconomical, since the optimal feed ratio is typically two or more times the minimum value.
2. For each candidate entrainer, start by assuming that the light component is the distillate (put it at the "product" vertex of the standard orientation) and then, starting at the cutoff value of Fr, use a continuation method to follow the *SN* fixed-point branch from the azeotrope and a large reflux ratio to a limit point and beyond at lower relux ratios, continuing until it is clear which saddle forms the limit point with *SN*.

(a) If *SN* forms a limit point with *S*1, then the correct component was selected as the distillate and Fr_{min} for this entrainer is below the cutoff value. Use two-parameter continuation to calculate the minimum feed ratio for this entrainer.

(b) If *SN* forms a limit point with *S*2, then either $Fr < Fr_{min}$ or the wrong component was selected as the distillate: pick the intermediate-boiling component to be the distillate (place it at the "product" vertex) and track the *SN* fixed-point branch as described above; if *SN* forms a limit point with *S*1, repeat step a; if *SN* forms a limit point with *S*2, Fr_{min} for this entrainer is greater than the cutoff value. Discard this entrainer.

After all the candidate entrainers have been examined, those entrainers with high minimum feed ratios (such as *sec*-butanol for separating methanol and MEK) will have been eliminated from further consideration, and only those entrainers with minimum feed ratios below the original cutoff point remain. These are then ranked according to their known minimum feed ratios. Of course, the design engineer must also consider such factors as the cost, toxicity, availability, corrosiveness and recoverability of the entrainer, possible chemical reactions, and the presence of severe tangent pinches (as in the methanol-acetone-MEK separation) when choosing the final entrainer. Thus, the entrainer with the lowest value of Fr_{min} may not be the best one, but the best entrainer should be among those remaining after the second-level screening of the feasible entrainers. Detailed design and economic studies can then be carried out for the one or two final-choice entrainers.

The calculations involved in determining r_{max}, Fr_{min}, and the product component are neither overly complicated nor overly time-consuming. All the computations in this article were carried out using standard numerical methods and the commercially-available continuation software package AUTO (Doedel, 1986). The CPU time required for these calculations is not prohibitive and does *not* make calculating the r_{max} vs. Fr branch, and Fr_{min} impractical for industrial applications. For example, calculating the r_{max} branch between $Fr = 1.0$ and $Fr = 0.1143$, and locating Fr_{min} in the acetone-methanol-water example can be done in as little as 15 min of CPU time on a VAXSTATION 3100 and in less than 4 min on a VAX 8830.

The ideas and methods presented here, in combination with previously existing methods, often make it possible to arrive at a good entrainer and a good set of design parameters for extractive distillation columns without performing any design calculations. First, the methods of Foucher et al. (1991) can be used to obtain a group of feasible extractive entrainers that give the residue-curve map in Figure 5. Then, given a reliable VLE model and the azeotropic feed composition, (1) set the entrainer feed to nearly pure entrainer (see pp. 164–165 of Knight, 1986, for the minimum purity), (2) set the desired product purities, $x_{D,1}$ and $x_{B,1}$, (3) set $x_{D,3}$ to a small number (10^{-10} to 10^{-15}) per Julka and Doherty (1990a), and (4) set q_U to a reasonable value, say 1.1 to 1.5. With only this information, (1) the product component can be determined for every feasible entrainer, (2) r_{max} can be calculated as a function of the feed ratio for every feasible entrainer, (3) Fr_{min} can be determined for every candidate entrainer, (4) the number of candidate extractive entrainers can be reduced by comparing Fr_{min} values to weed out those uneconomical entrainers requiring large feed ratios, (5) an estimate of a reasonable range of operating feed ratios can be made, (6) minimum reflux can be calculated as a function of the feed ratio by using the fixed-point-tracking approach of Julka and Doherty (1993) and Fidkowski et al. (1991), (7) a good design value of the reflux can be picked up by setting $r_{op} = 1.2\text{–}1.5\ r_{min}$, and (8) an estimate of the range of operating reflux ratios ($r_{max} - r_{min}$) can be made. At this point, one would have a good initial set of values for some of the major design parameters for two or three of the most promising entrainers to separate the azeotropic mixture. Then, and only then, do the column design calculations begin. Thus, the techniques presented in this article should speed up and improve the synthesis and design of extractive distillation separation systems.

Conclusions

In addition to a minimum reflux ratio, every extractive distillation also exhibits a maximum reflux ratio above which the desired separation is impossible and a minimum entrainer flow rate (expressed as a ratio of the two feed streams) below which the separation is also impossible. The fixed points of the finite-difference equations describing the middle section of the column hold the key to understanding both of these phenomena. In the normal range of operating feed ratios, maximum reflux corresponds to *two* of the middle-section fixed points meeting at a limit point and eliminating each other. The minimum feed ratio corresponds to a bifurcation point where *three* of the middle-section fixed points meet. The fixed points of the middle-section map exhibit the perturbations of the standard pitchfork bifurcation. The maximum reflux ratio and the minimum feed ratio represent two of these perturbations. Both quantities are easily calculated using commercially available arc-length continuation software packages *before* starting any column design calculations.

As invaluable as residue-curve maps are for identifying feasible extractive entrainers, they are not sufficient for selecting entrainers that result in practical, economical designs. Because the feed ratio is one of the variables with the greatest effect on the cost of an extractive distillation sequence, feasible entrainers with very large minimum feed ratios will not be economical. An algorithm is presented for screening the set of feasible entrainers by identifying and discarding those clearly uneconomical entrainers with large minimum feed ratios. A significant advantage of this approach is that the list of candidate entrainers can be reduced to the two or three most promising ones without the need for any column design calculations. After reducing the number of candidate entrainers, guidelines are presented for making a good initial guess for the design value of the feed ratio for each remaining entrainer.

The presence of a maximum reflux ratio has important implications for the operation and control of extractive distillations. The number of trays required for a given separation becomes infinite at both the minimum and the maximum reflux ratios. Thus, at low reflux ratios, an increase in the reflux will improve the degree of separation, while at larger reflux ratios an increase in reflux causes a decrease in the degree of separation. After the column is built, the number of trays is obviously fixed. Therefore, if the number of trays required to achieve a desired separation increases beyond the number built into the column, the amount of separation must decrease. Consequently, the control system must know when to increase and when to decrease the internal flows to maintain the product purities. The operation and control of extractive columns become easier at larger feed ratios, because the maximum reflux ratio increases with feed ratio.

Depending on the entrainer, the intermediate-boiling pure component sometimes becomes the pure product leaving the extractive column. This is a strictly thermodynamic effect caused by the influence of the entrainer on the relative volatilities of the constituents of the original azeotropic mixture and therefore can always be determined before starting to design an extractive distillation sequence either by examining the behavior of the fixed points of the middle-section map, by drawing a series of pseudo-binary phase diagrams, or by the method of Laroche et al. (1991).

A completely analogous theory exists for the extractive distillation of maximum-boiling azeotropes (Knapp, 1991).

Acknowledgment

This research was partially supported by the National Science Foundation (Grant No. NSF-CTS-91-13717). The authors wish to thank Professor M. P. Harold of the University of Massachusetts for his helpful discussions on singularity theory and Professor M. Morari and L. Laroche of CalTech for bringing the methanol-MEK-*sec*-butanol example to our attention. We are grateful to Ms. Pamela Stephan for preparing the figures.

Notation

A = arbitrary $m \times n$ matrix
A^T = transpose of a matrix A
$\mathcal{B}$ = bifurcation variety
B = bottom stream or bottoms flow rate
C = number of components in a mixture
D = distillate stream or flow rate
$\underline{f}$ = fixed-point equation (middle-section fixed-point equation in Eqs. 15 to 18)
F = overall feed stream or flow rate
F_L = lower feed or feed flow rate
Fr = feed ratio, F_U/F_L, for direct splits
$Fr_{\mathcal{H}}$ = feed ratio at which a hysteresis point occurs in a (r, Fr) plot (equivalent to crossing $\mathcal{H}$)
$Fr_{\min}$ = minimum feed ratio
F_U = upper feed or feed flow rate
$h(Fr, \underline{w})$ = function defined by Eq. A9 that depends only on the feed ratio and feed and product compositions
$\mathcal{H}$ = hysteresis variety
I = identity matrix
J = Jacobian matrix with respect to the state variables
L_B = molar liquid-phase flow rate in the bottom (stripping) section of a column
L_M = molar liquid-phase flow rate in the middle section of a column
L_T = molar liquid-phase flow rate in the top (rectifying) section of a column
P_i^{sat} = vapor pressure of component i
q_L = lower-feed quality
q_U = upper-feed quality
r = reflux ratio
r_M = middle-section reflux ratio
$r_{\max}$ = maximum reflux ratio
$r_{\min}$ = minimum reflux ratio
s = reboil ratio
SN = stable node originating at the azeotrope
SN^- = stable node originating outside the composition simplex
$S1$ = saddle originating at the "product" vertex
$S2$ = saddle originating at the "nonproduct" vertex
$\underline{u}$ = column vector of state variables
UN = unstable node originating at the entrainer vertex
UN^- = unstable node originating outside the composition simplex
V_B = molar vapor-phase flow rate in the bottom (stripping) section of a column
V_M = molar vapor-phase flow rate in the middle section of a column
V_T = molar vapor-phase flow rate in the top (rectifying) section of a column
$\underline{w}$ = vector of feed and product mole fractions defined by Eq. A9
x = liquid-phase composition (mole fraction)
$\underline{x}$ = column vector of liquid-phase mole fractions (dimension C-1)
$\underline{x}_B$ = column vector of bottom compositions (dimension C-1)
$\underline{x}_D$ = column vector of distillate compositions (dimension C-1)
$\underline{x}_{F_L}$ = column vector of lower-feed compositions (dimension C-1)

$\underline{x}_{F_U}$ = column vector of upper-feed compositions (dimension C-1)
y = vapor-phase composition (mole fraction)
$\underline{y}$ = column vector of vapor-phase mole fractions (dimension C-1)
Y = matrix of derivatives of the vapor mole fractions with respect to the liquid mole fractions at constant pressure with C-2 mole fractions held constant for each derivative
Y_{ij} = $[\partial y_i/\partial x_j]_{P,\underline{x}}$
$\underline{z}_F$ = column vector of overall-feed compositions (dimension C-1)

Greek letters

α_{ij} = volatility of component i relative to component j
$\underline{\alpha}$ = vector of parameters in the system of equations in Eq. 13
α, β = parameters in the universal unfolding of the pitchfork singularity
δ = multiplier of $Fr_{\min}$ in the heuristic for an operating value of the feed ratio (Eq. 24)
γ_i = activity coefficient of component i
λ = bifurcation parameter
σ = multiplier of $Fr_{\min}$ in the heuristic for the economically optimal value of the feed ratio (Eq. 23)

Superscripts

m = middle section or middle-section map
r = rectifying section or rectifying map
s = stripping section or stripping map
$\hat{}$ = fixed point

Subscripts

heavy = heavy (least volatile) component
i = component i
k = tray number in the middle section
light = light (most volatile) component
m = tray number in the rectifying section
n = tray number in the stripping section
N = last tray in the stripping section (integer)
op = operating value
optimum = optimal value

Literature Cited

Andersen, H. W., L. Laroche, and M. Morari, "Effect of Design on the Control of Homogeneous Azeotropic Distillations," AIChE Meeting, San Francisco (Nov., 1989).

Berg, L., "Azeotropic and Extractive Distillation ... Selecting the Agent for Distillation Processes," *Chem. Eng. Prog.*, **65**, 52 (1969).

Berg, L., and An-I. Yeh, "Separation of Methanol from Acetone by Extractive Distillation," U.S. Patent No. 4,501,645 (Feb. 26, 1985a).

Berg, L., and An-I. Yeh, "The Unusual Behavior of Extractive Distillation: Reversing the Volatility of the Acetone-Isopropyl Ether System," *AIChE J.*, **31**, 504 (1985b).

Berg, L., and An-I. Yeh, "Dehydration of Ethanol by Extractive Distillation," U.S. Patent No. 4,631,115 (Dec. 23, 1986).

Berg, L., and An-I. Yeh, "Dehydration of Ethanol by Extractive Distillation," U.S. Patent No. 4,654,123 (Mar. 31, 1987).

Bernot, C., M. F. Doherty, and M. F. Malone, "Patterns of Composition Change in Multicomponent Batch Distillation," *Chem. Eng. Sci.*, **45**, 1207 (1990).

Black, C., "Distillation Modeling of Ethanol Recovery and Dehydration Processes for Ethanol and Gasohol," *Chem. Eng. Prog.*, **76**(9), 78 (1980).

Buell, C. K., and R. G. Boatright, "Furfural Extractive Distillation," *Ind. Eng. Chem.*, **39**, 695 (1947).

Doedel, E., "AUTO: Software for Continuation and Bifurcation Problems in Ordinary Differential Equations," Dept. of Mathematics, Calif. Inst. of Technol., Pasadena (1986).

Doherty, M. F., and G. A. Caldarola, "Design and Synthesis of Homogeneous Azeotropic Distillations: 3. The Sequencing of Columns for Azeotropic and Extractive Distillations," *Ind. Eng. Chem. Fund.*, **24**, 474 (1985).

Doherty, M. F., and J. D. Perkins, "On the Dynamics of Distillation Processes: I. The Simple Distillation of Multicomponent Non-Reacting, Homogeneous Liquid Mixtures," *Chem. Eng. Sci.*, **33**, 281 (1978).

Ewell, R. H., J. M. Harrison, and L. Berg, "Azeotropic Distillation," *Ind. Eng. Chem.*, **36**, 871 (1944).

Fidkowski, Z. T., M. F. Malone, and M. F. Doherty, "Nonideal Multicomponent Distillation: Use of Bifurcation Theory for Design," *AIChE J.*, **37**, 1761 (1991).

Foucher, E. R., M. F. Doherty, and M. F. Malone, "Automatic Screening of Entrainers in Homogeneous Azeotropic Distillation," *Ind. Eng. Chem. Res.*, **30**, 760 (1991).

Golubitsky, M., and D. Schaeffer, "A Theory for Imperfect Bifurcation via Singularity Theory," *Commun. Pure Appl. Math.*, **32**, 21 (1979).

Golubitsky, M., and D. G. Schaeffer, *Singularities and Groups in Bifurcation Theory*, Vol. I, Springer-Verlag, New York (1985).

Jacobsen, E. W., L. Laroche, M. Morai, S. Skogestad, and H. W. Andersen, "Robust Control of Homogeneous Azeotropic Distillation Columns," *AIChE J.*, **37**, 1810 (1991).

Julka, V., "A Geometric Theory of Multicomponent Distillation," PhD Diss., Univ. of Massachusetts, Amherst (1993).

Julka, V., and M. F. Doherty, "Geometric Behavior and Minimum Flows for Nonideal Multicomponent Distillation," *Chem. Eng. Sci.*, **45**, 1801 (1990a).

Julka, V., and M. F. Doherty, "A Geometric Analysis of Nonideal Multicomponent Distillation with Nonsharp Splits," AIChE Meeting, Chicago (Nov., 1990b).

Julka, V., and M. F. Doherty, "Geometric Nonlinear Analysis of Multicomponent Nonideal Distillation: A Simple Computer-Aided Design Procedure," *Chem. Eng. Sci.*, **48**, 1367 (1993).

Knapp, J. P., "Exploiting Pressure Effects in the Distillation of Homogeneous Azeotropic Mixtures," PhD Diss., Univ. of Massachusetts, Amherst (1991).

Knapp, J. P., and M. F. Doherty, "Thermal Integration of Homogeneous Azeotropic Distillation Sequences," *AIChE J.*, **36**, 969 (1990).

Knapp, J. P., and M. F. Doherty, "A New Pressure-Swing Distillation Process for Separating Homogeneous Azeotropic Mixtures," *Ind. Eng. Chem. Res.*, **31**, 346 (1992).

Knight, J. R., "Synthesis and Design of Homogeneous Azeotropic Distillation Sequences," PhD Diss., Univ. of Massachusetts, Amherst (1986).

Knight, J. R., and M. F. Doherty, "Design and Synthesis of Homogeneous Azeotropic Distillations: 5. Columns with Nonnegligible Heat Effects," *Ind. Eng. Chem. Fund.*, **25**, 279 (1986).

Knight, J. R., and M. F. Doherty, "Optimal Design and Synthesis of Homogeneous Azeotropic Distillation Sequences," *Ind. Eng. Chem. Fund.*, **28**, 564 (1989).

Koehler, J. W., P. Aguirre, and E. Blass, "Minimum Reflux Calculations for Nonideal Mixtures Using the Reversible Distillation Model," *Chem. Eng. Sci.*, **46**, 3007 (1991).

Kolbe, B., J. Gmehling, and U. Onken, "Selection of Solvents for Extractive Distillation Using Predicted and Correlated VLE Data," *Inst. Chem. Eng. Symp. Ser.*, No. 56, 1.3/23 (1979).

Laroche, L., N. Bekiaris, H. W. Andersen, and M. Morari, "Homogeneous Azeotropic Distillation: Comparing Entrainers," *Can. J. Chem. Eng.*, **69**, 1302 (1991).

Levy, S. G., D. B. Van Dongen, and M. F. Doherty, "Design and Synthesis of Homogeneous Azeotropic Distillations: 2. Minimum Reflux Calculations for Nonideal and Azeotropic Columns," *Ind. Eng. Chem. Fund.*, **24**, 463 (1985).

Levy, S. G., and M. F. Doherty, "Design and Synthesis of Homogeneous Azeotropic Distillations: 4. Minimum Reflux Calculations for Multiple-Feed Columns," *Ind. Eng. Chem. Fund.*, **25**, 269 (1986a).

Levy, S. G., and M. F. Doherty, "A Simple Exact Method for Calculating Tangent Pinch Points in Multicomponent Nonideal Mixtures by Bifurcation Theory," *Chem. Eng. Sci.*, **41**, 3155 (1986b).

Matsuyama, H., and H. Nishimura, "Topological and Thermodynamic Classification of Ternary Vapor-Liquid Equilibria," *J. Chem. Eng. Japan*, **10**, 181 (1977).

Robinson, C. S., and E. R. Gilliland, *Elements of Fractional Distillation*, 4th ed., McGraw-Hill, New York (1950).
Scheibel, E. G., "Principles of Extractive Distillation," *Chem. Eng. Prog.*, **44**, 927 (1948).
Scheintuch, M., and D. Luss, "Application of Singularity Theory to Modeling of Steady-State Multiplicity: Propylene Oxidation on Platinum," *Ind. Eng. Chem. Fund.*, **22**, 209 (1983).
Stichlmair, J. G., and J-R. Herguijuela, "Separation Regions and Processes of Zeotropic and Azeotropic Ternary Distillation," *AIChE J.*, **38**, 1523 (1992).
Strang, G., *Introduction to Applied Mathematics*, Wellesley-Cambridge Press, Wellesley, MA (1986).
Wahnschafft, O. M., J. W. Koehler, E. Blass, and A. W. Westerberg, "The Product Composition Regions of Single-Feed Azeotropic Distillation Columns," *Ind. Eng. Chem. Res.*, **31**, 2345 (1992).
Yeh, An-I, L. Berg, and K. J. Warren, "The Separation of Acetone-Methanol Mixture by Extractive Distillation," *Chem. Eng. Commun.*, **68**, 69 (1988).
Zudkevitch, D., S. E. Belsky, and P. D. Krautheim, "Extraction and/or Extractive Distillation of Low Molecular Weight Alcohols from Aqueous Solutions," U.S. Patent No. 4,428,798 (Jan. 31, 1984a).
Zudkevitch, D., D. K. Preston, and S. E. Belsky, "Extraction and/or Extractive Distillation of Ethanol from Aqueous Solutions," U.S. Patent No. 4,455,198 (June 19, 1984b).

Appendix A: Model Derivation

The finite-difference equations describing the middle-section for direct splits are derived here. The notation is shown in Figure 1. Because there are C-1 independent mole fractions, all composition vectors are (C-1)-dimensional.

The two feed flow rates are expressed as the feed ratio:

$$Fr \equiv \frac{F_U}{F_L} = \frac{\text{Entrainer Flow Rate}}{\text{Feed Flow Rate}} \tag{A1}$$

which allows the definition of an overall feed flow rate and feed composition:

$$F = F_U + F_L = F_L(Fr+1) \tag{A2}$$

$$\underline{z}_F = \frac{Fr\underline{x}_{F_U} + \underline{x}_{F_L}}{Fr+1} \tag{A3}$$

Mass balances around the entire column then become:

$$F = F_U + F_L = D + B \tag{A4}$$

$$F\underline{z}_F = F_U\underline{x}_{F_U} + F_L\underline{x}_{F_L} = D\underline{x}_D + B\underline{x}_B \tag{A5}$$

Equations A1 to A5 can be rearranged to give:

$$\frac{z_{F,i} - x_{B,i}}{z_{F,1} - x_{B,1}} = \frac{z_{F,i} - x_{D,i}}{z_{F,1} - x_{D,1}} \quad (i = 2,\ C\text{-}1) \tag{A6}$$

$$\frac{D}{B} = \frac{z_{F,i} - x_{B,i}}{x_{D,i} - z_{F,i}} \tag{A7}$$

$$\frac{F_L}{B} = \frac{x_{D,i} - x_{B,i}}{Fr(x_{D,i} - x_{F_U,i}) + x_{D,i} - x_{F_L,i}} \tag{A8}$$

$$\frac{F_U}{D} = \frac{Fr(x_{D,i} - x_{B,i})}{Fr(x_{F_U,i} - x_{B,i}) + x_{F_L,i} - x_{B,i}} = h(Fr,\ \underline{w}) \tag{A9}$$

where F_U/D has been expressed as $h(Fr,\ \underline{w})$ to indicate its dependence on the feed ratio and the composition of the feed, distillate, and bottoms. (The elements of the vector $\underline{w}$ are $x_{F_U,i}$, $x_{F_L,i}$, $x_{D,i}$, and $x_{B,i}$).

For CMO columns, the feed quality, q, is simply the molar fraction of the feed that is liquid. Therefore, the internal flow rates of the three column sections can be related by:

$$L_M = L_T + q_U F_U \tag{A10}$$

$$L_M = L_B - q_L F_L \tag{A11}$$

$$V_M = V_T - (1 - q_U)F_U \tag{A12}$$

$$V_M = V_B + (1 - q_L)F_L \tag{A13}$$

A mass balance around the top half of the column cut at middle-section tray $k+1$ (see Figure 1) gives:

$$L_M\underline{x}^m_{k+1} + D\underline{x}_D = V_M\underline{y}^m_k + F_U\underline{x}_{F_U} \tag{A14}$$

Using Eqs. 2, 3, A10 and A12, Eq. A14 becomes the middle-section finite-difference equation, Eq. 7a.

The relationship between the reflux and reboil ratios given in Eq. 8 can be derived either from Eqs. 2, 6, A10 and A11 or from Eqs. 3, 5, A12 and A13.

Note that, even though this article deals only with the extractive distillation of ternary mixtures, the model equations are valid for the distillation of any C-component mixture in a double-feed column. (Indirect splits are better described by the equations given in Knapp, 1991.)

Appendix B: Behavior at Large Feed Ratios

The standard r_{max} behavior (the formation of a limit point between the $S1$ and SN branches) always occurs in the neighborhood of Fr_{min}, usually continues through the range of normal operating feed ratios, and can persist to very high multiples of Fr_{min}. For example, the SN-$S1$ limit point continues to exist at $110Fr_{min}$ in the ethanol-water-ethylene glycol separation and beyond $40Fr_{min}$ in the methanol-MEK-*sec*-butanol example. This, however, is not true for all separations. At $8.86Fr_{min}$ in the acetone-methanol-water example and $11.6Fr_{min}$ in the separation of a proprietary mixture, the $S1$ and SN fixed-point branches cease forming a limit point with each other. A maximum reflux still exists at higher feed ratios, but now it is caused by a different phenomenon. At such "large" feed ratios, the SN branch moves first to the base of the triangle and then along it. Under these conditions, r_{max} is the reflux ratio at which the SN branch just crosses the rectifying profile. Apparently, every separation undergoes this transition in the defining condition of r_{max} at sufficiently large feed ratios.

Consider the limiting case of infinite feed ratio. After some algebra, Eqs. A2 to A14, 7, 8 and 11, which describe a double-feed column, reduce to the corresponding equations for a single-feed column, and the equations describing the middle section become the stripping-section equations (Eqs. 4-6 and 10). Less formally, the same conclusion is reached by realizing that $Fr \to \infty$ is the same as letting $F_L \to 0$ in Eq. A1. If the lower-feed flow rate is zero, F_U becomes the only feed, and there is no longer any distinction between the stripping and middle

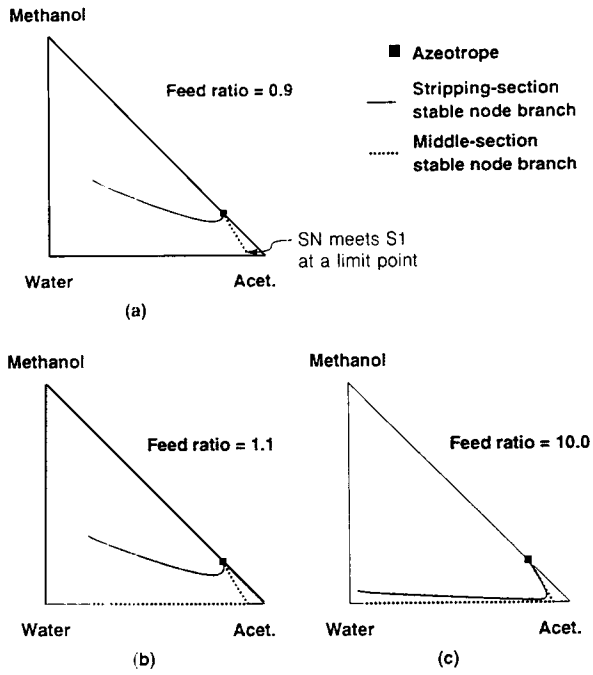

Figure B1. Behavior of the stable node branches in the middle and stripping sections as a function of *Fr*.

(a) Middle-section *SN* branch exhibits the standard r_{max} behavior at $Fr = 0.09$. The stable-node branches in the stripping and middle sections do not show any similarity; (b) New r_{max} behavior by $Fr = 1.1$. The middle-section stable node branch starts to resemble the stripping-section stable node branch; (c) By $Fr = 10$ the similarity between the stripping and middle sections is apparent.

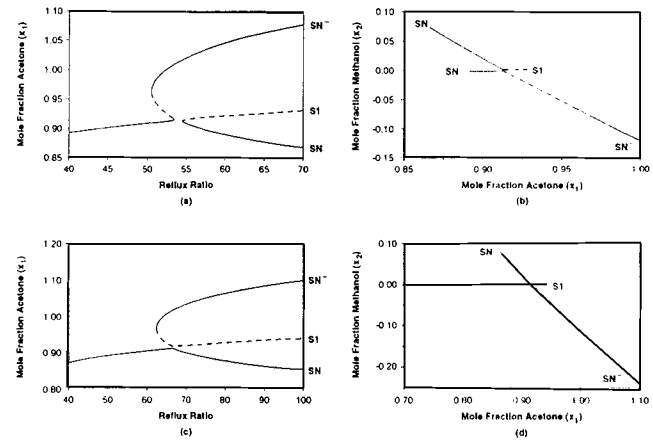

Figure B2. Perturbed pitchfork bifurcation between the *SN*, *S1*, and *SN*⁻ fixed-point branches which causes the transition to the nonstandard r_{max} behavior (acetone-methanol-water separation).

(a) The (x_1, r) projection of the standard r_{max} behavior at $Fr = 0.90$; (b) The (x_1, x_2) projection at $Fr = 0.90$; (c) The (x_1, r) projection of the nonstandard r_{max} behavior at $Fr = 1.1$; (d) The (x_1, x_2) projection at $Fr = 1.1$.

sections. This result is completely general and therefore applies equally to the ethanol-water-ethylene glycol and acetone-methanol-water separations, despite their seemingly different behaviors at large feed ratios.

Figure B1 shows how the behavior of the middle-section map approaches that of the stripping map as the feed ratio becomes large, by comparing the branch of stable nodes (originating from the azeotrope) for the stripping and middle sections of the acetone-methanol-water separation. At $Fr = 0.9$ (Figure B1a) the middle-section stable-node branch (*SN*) coalesces with the *S1* branch at a limit point at $r = 54.57$. This is the standard r_{max} behavior. The stripping-section stable-node branch behaves quite differently. It moves in the opposite direction across the triangle and forms no limit point. By $Fr = 1.1$ (Figure B1b), the *SN* branch has completely changed. It no longer forms a limit point with *S1*, but instead continues to the base of the composition triangle (crossing the rectifying profile) and then moves along the triangle base toward the entrainer vertex. This is the fixed-point branch behavior that gives rise to the new, nonstandard type of maximum reflux ratio. Now there is some similarity between the shapes of the middle- and stripping-section stable-node branches. At $Fr = 10.0$ (Figure B1c), the stable node branches for the stripping and middle sections closely resemble each other in both shape and position. These two branches get closer and closer at larger feed ratios. Since all extractive distillations must end up with the middle section being equivalent to the stripping section at $Fr \to \infty$, it follows that all extractive distillations undergo the transition in the defining condition of maximum reflux at some sufficiently large feed ratio.

At some specific feed ratio, there is a sudden switch from the formation of a limit point between the *S1* and *SN* branches to no limit point between *S1* and *SN*. Instead, as shown in Figure B1b, the *SN* branch continues to the triangle base and then moves along it. Maximum reflux now corresponds to the reflux ratio at which the *SN* branch first crosses the rectifying profile. This nonstandard r_{max} value is more difficult to calculate because it requires knowledge of the location of the rectifying profile at each reflux ratio, whereas the standard maximum reflux does not. Note that the *SN* branch, not the SN^- branch, is the branch of attracting fixed points for feasible extractive columns in the region of nonstandard r_{max} behavior. Also, the saddle *S1* and its separatrices are no longer a contributing factor to maximum reflux. Despite the sudden change in fixed-point branch behavior, the transition between the two types of maximum reflux is smooth. There is no sudden jump in the value of r_{max} nor any noticeable discontinuity in the parameters of a feasible column design (such as the number of trays in each column section).

Throughout most of the text, the emphasis has been on the behavior of the *S1*, *S2*, and *SN* fixed-point branches. This was sufficient to understand both the minimum entrainer flow and the standard maximum reflux phenomena, but the explanation of the transition to the nonstandard r_{max} behavior requires the SN^- branch as well. The cause of the transition is simply another pitchfork bifurcation, but this one involves the *SN*, *S1*, and SN^- branches. Figure B2 illustrates the switch in r_{max} behavior for the acetone-methanol-water separation. At $Fr = 0.90$, the standard type of maximum reflux exists; *S1* and *SN* form a limit point (Figure B2a). Note that the SN^- branch contains a hysteresis loop. Figure B2b is a magnified view of the corresponding (x_1, x_2) fixed-point-branch projection. Note how close the SN^- branch comes to the *SN*-*S1* limit point before starting to move along the base of the composition

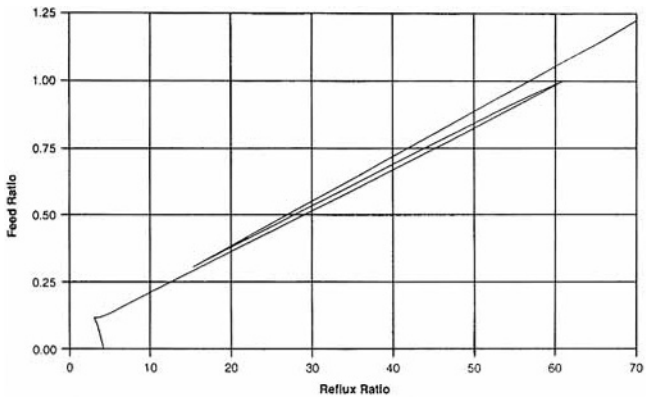

Figure B3. Cusps summarizing the behavior of the *S1*, *S2*, *SN*, and *SN*⁻ fixed-point branches for the acetone-methanol-water separation.

triangle. Figure B2c indicates that the nonstandard maximum reflux behavior has started by $Fr = 1.1$. *SN* no longer forms a limit point with *S1*. Instead, SN^- and *S1* form a limit point. Comparing parts *a* and *c* of Figure B2 with Figure 16, it is clear that, as the feed ratio increases, the *SN*, *S1*, and SN^- fixed-point branches exhibit the pitchfork bifurcation perturbations consistent with bifurcation diagrams (d), (c), and (a) in Figure 16. (The stability of the fixed-point branches in Figure 16 must be reversed and the branch labels must be changed from *S1*, *SN*, and *S2* to SN^-, *S1*, and *SN*, respectively, to make the comparison exact.) The transition point between the two types of maximum reflux behavior, where *SN*, *S1*, and SN^- all meet at a single point, corresponds to the perturbed pitchfork shown in Figure 16(a-c). Figure B2d shows the (x_1, x_2) projection of the data in Figure B2c. Note how the *SN* branch moves all the way to the base of the composition triangle and then moves along it, as shown in Figure B1b, and that the *S1*-SN^- limit point lies outside the composition state space. The location of the transition to the nonstandard r_{max} behavior depends very strongly on the product purity. As the mole fraction of acetone in the distillate decreases from 0.995 to 0.95, the transition point moves from $Fr = 1.00$ to $Fr \sim 46$.

Just like in the calculation of Fr_{min}, two-parameter continuation can be used to locate the bifurcation point signalling the end of the standard r_{max} behavior. In practice, this would seldom be done since the transition point usually occurs above the normal range of operating feed ratios, knowledge of its location does not influence the column design, and large amounts of computer time are often necessary when the transition occurs at a high feed ratio.

The cusps shown in Figures 18d, 19e, 20e, 22e, 23 and 24 show only the behavior of the *S1*, *S2* and *SN* fixed-point branches. Though it is not necessary from a design engineer's perspective, the other fixed-point branches can also be tracked and plotted in (r, Fr) space. Figure B3 shows the resulting plot for the acetone-methanol-water separation. This figure can easily be related to the corresponding bifurcation diagrams by taking slices at constant feed ratio. Each point on the curve represents a limit, bifurcation, or hysteresis point. For $Fr > 1.004$, there is only one limit point, the one between *S1* and SN^- (see Figure B2c). At $Fr = 1.004$, a bifurcation occurs between *S1*, *SN*, and SN^- and the *S1*-SN^- limit point becomes a limit point on the SN^- branch. The bifurcation diagram has the structure of Figure 16(a-c) with the branch stability reversed and the branch labels changed. This is the transition point between the standard and nonstandard maximum reflux behaviors. For all feed ratios between 1.004 and 0.300, there are three limit points. Reading left-to-right across the figure, the first two limit points are on the SN^- branch (the SN^- branch has a hysteresis loop), while the third limit point is between *S1* and *SN*, and it determines r_{max}. Figure B2a is representative of a bifurcation diagram in this range. At $Fr = 0.300$, the two limit points on the SN^- branch coalesce at a hysteresis point. From here on the explanation is the same as for the cusp shown in Figure 18d. Hysteresis in the *S2* branch starts at $Fr_{HC} = 0.1143$, and the *S1*, *S2*, and *SN* branches meet at a bifurcation point at $Fr_{min} = 0.1133$. More complicated behavior can occur in other mixtures, but the behavior is always decipherable in terms of limit, bifurcation and hysteresis points on the various fixed-point branches. For example, in the methanol-acetone-MEK separation, the *S1*, *S2*, *SN*, SN^-, and *UN* fixed-point branches meet in different combinations at limit points and bifurcation points, plus the SN^- and *S2* branches exhibit hysteresis loops.

Manuscript received Nov. 30, 1992, and revision received June 14, 1993.